SUPPORTING INFORMATION FOR

Unity Fluorescent Carbene-Gold(I)-Acetylide Complexes with Two-Photon Absorption and Energy-Efficient Blue FOLED

Alexander C. Brannan, Hwan-Hee Cho, Jonathan Daniel, Nguyen Le Phuoc, Amelia Harvey, Charles T. Smith, Mikko Linnolahti, Mireille Blanchard-Desce,* Neil C. Greenham* and Alexander S. Romanov**

Supporting Information Table of Contents

GENERAL CONSIDERATIONS

All reactions were performed under a N_2 atmosphere. Solvents were dried as required. Reagents and catalysts were purchased from commercial vendors and used as received. (BiCAAC)AuCl was prepared according to the literature procedure.[1] ^{1}H and ^{13}C{^{1}H} NMR spectra were recorded using a Bruker AVIII HD 500 MHz NMR spectrometer. ^{1}H NMR spectra (500.19 MHz) and ^{13}C{^{1}H} (125.79 MHz) were referenced to CD_2Cl_2 at δ 5.32 (^{13}C, δ 53.84) and $CDCl_3$ at δ 7.26 (^{13}C, δ 77.16). IR spectra were recorded using a Bruker ALPHA FT-IR spectrometer equipped with a platinum ATR attachment. All electrochemical experiments were performed using an Autolab PGSTAT 302N computer-controlled potentiostat. Cyclic voltammetry (CV) was performed using a three-electrode configuration consisting of a glassy carbon macrodisk working electrode (GCE) (diameter of 3 mm; BASi, Indiana, U.S.A.) combined with a Pt wire counter electrode (99.99%; GoodFellow, Cambridge, U.K.) and an Ag wire pseudoreference electrode (99.99%; GoodFellow, Cambridge, U.K.). The GCE was polished between experiments using alumina slurry (0.3 μm), rinsed in distilled water and subjected to brief sonication to remove any adhering alumina microparticles. The metal electrodes were then dried in an oven at 100 °C to remove residual traces of water, the GCE was left to air dry and residual traces of water were removed under vacuum. The Ag wire pseudoreference electrodes were calibrated to the ferrocene/ferrocenium couple in THF at the end of each run to allow for any drift in potential, following IUPAC recommendations.[2] All electrochemical measurements were performed at ambient temperatures under an inert N_2 atmosphere in THF containing the complex under study (1.4 mM) and the supporting electrolyte [*n*-Bu_4N][PF_6] (0.13 M). Data were recorded with Autolab NOVA software (v. 1.11). Thermogravimetric analysis was performed by the Microanalysis Laboratory at the University of Manchester. Elemental analyses were performed by the Microanalysis Laboratory at the University of Manchester. Mass spectrometry data were obtained by the Mass Spectrometry Laboratory at the University of Manchester. Thermogravimetric analysis was performed with a TA Instruments SDT650 simultaneous thermal analyser under a stream of nitrogen.

Experimental.

Au1: ^{1}H NMR (500 MHz, CD_2Cl_2)

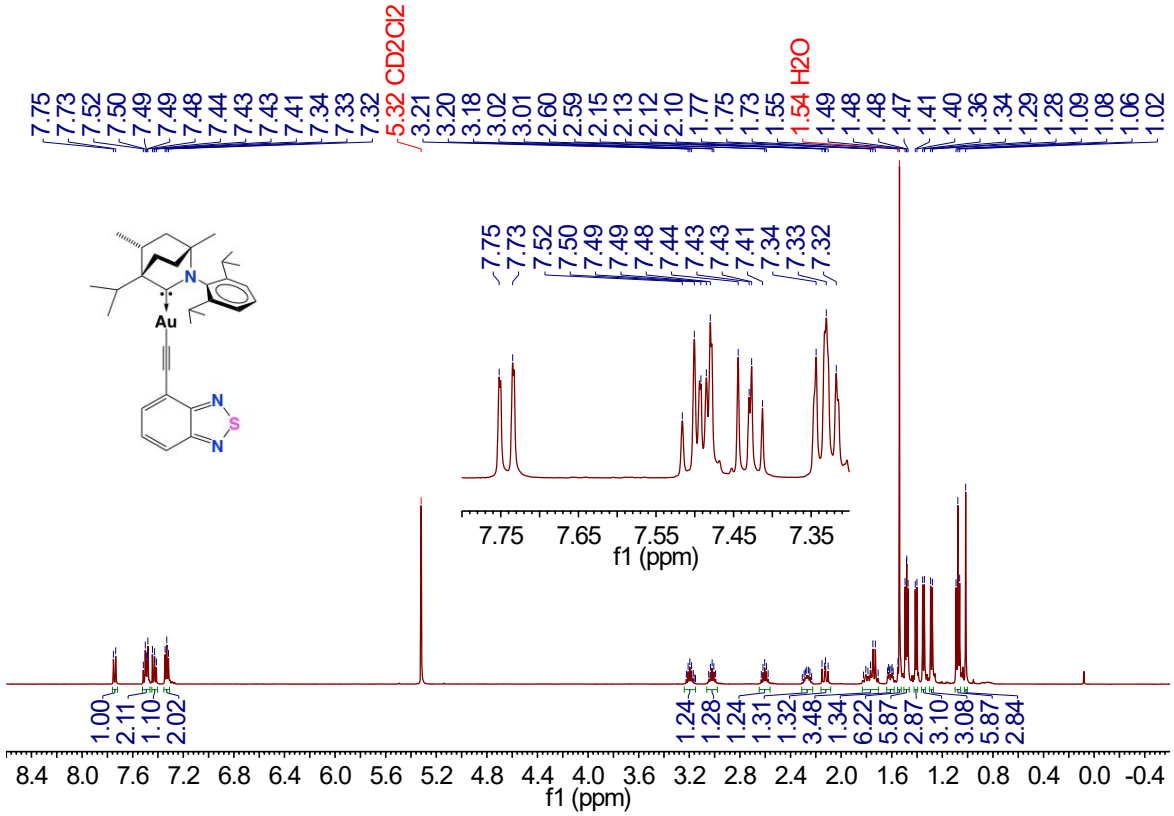

Au1: ^{13}C{^{1}H} NMR (126 MHz, CD_2Cl_2)

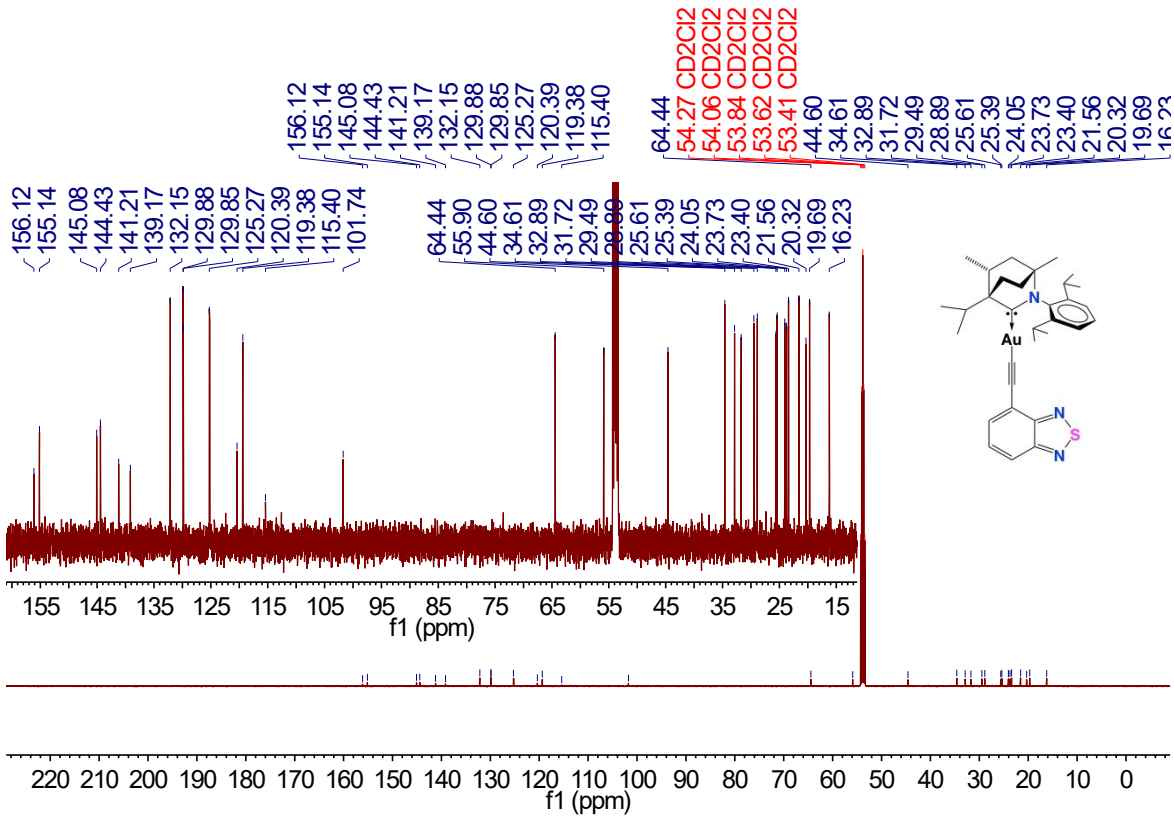

Au1: HMBC ^{1}H:$^{13}C\{^{1}H\}$ NMR (CD_2Cl_2)

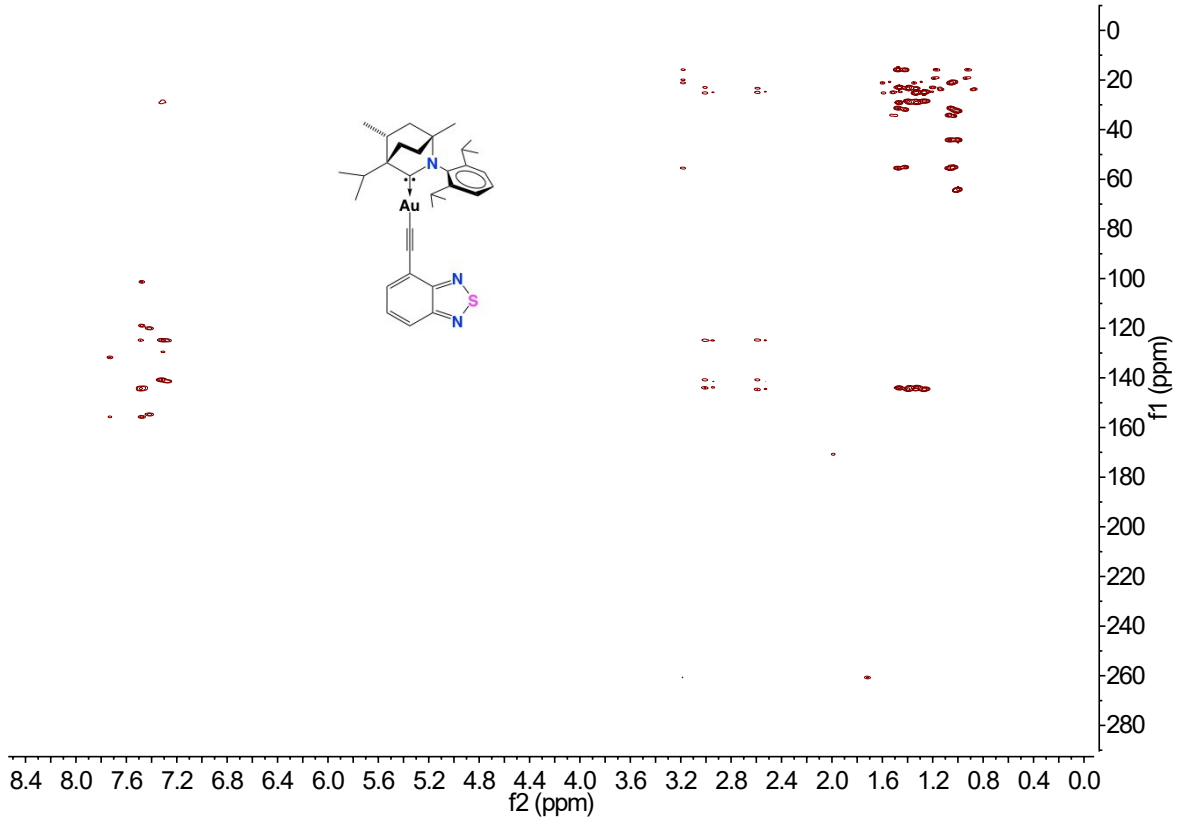

Au2: ^{1}H NMR (500 MHz, CD_2Cl_2)

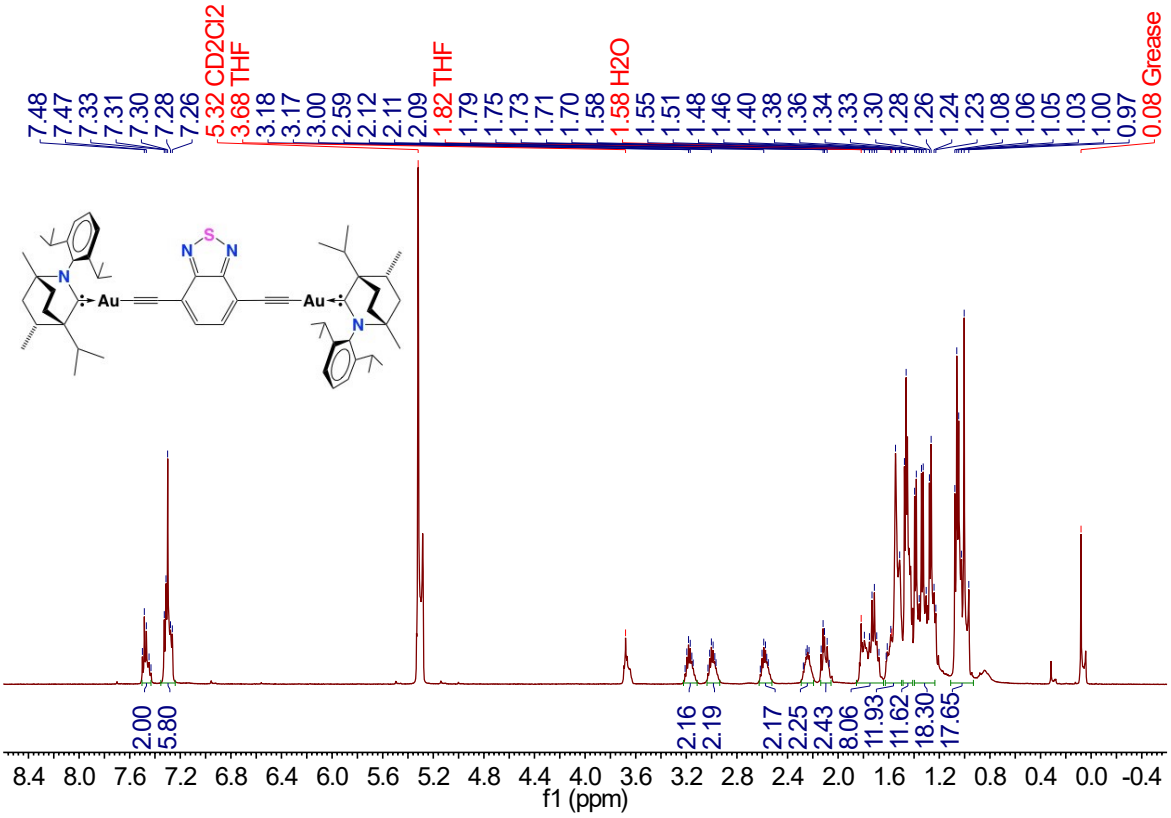

Au2: $^{13}C\{^{1}H\}$ NMR (125 MHz, CD_2Cl_2)

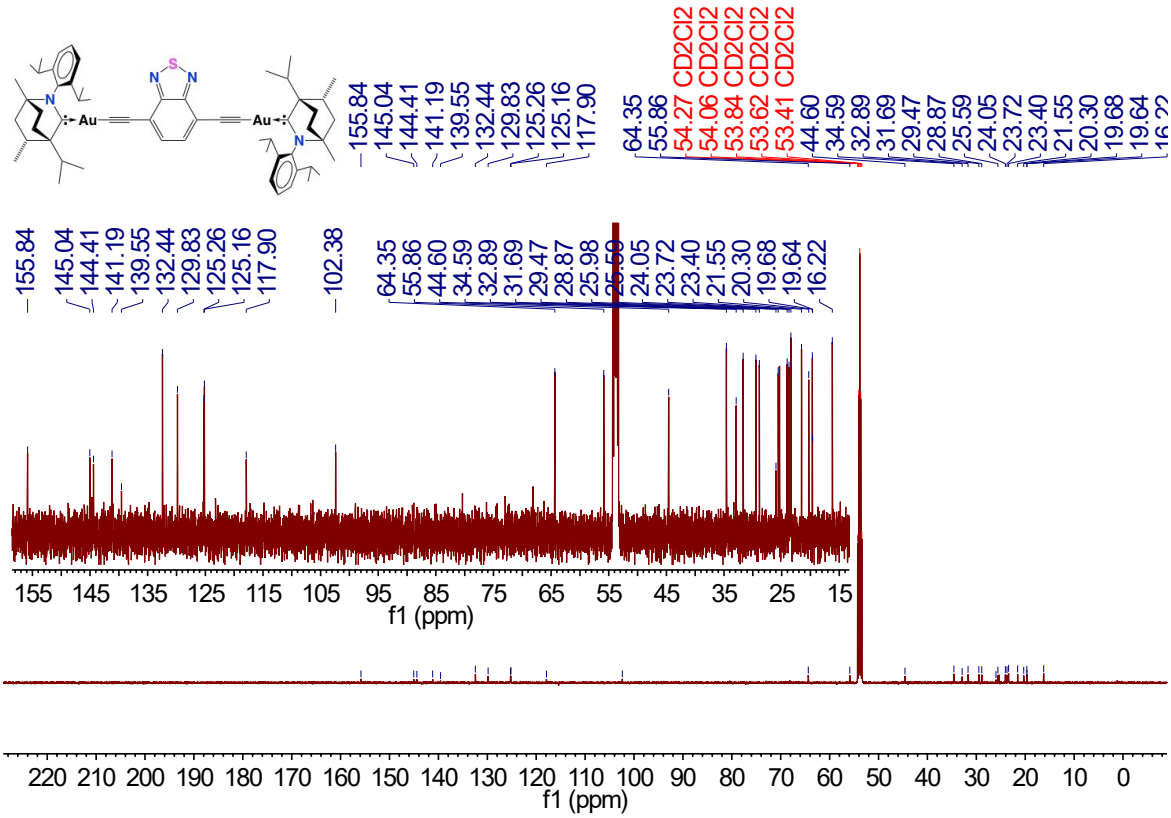

Au2: HMBC ^{1}H:$^{13}C\{^{1}H\}$ NMR (CD_2Cl_2)

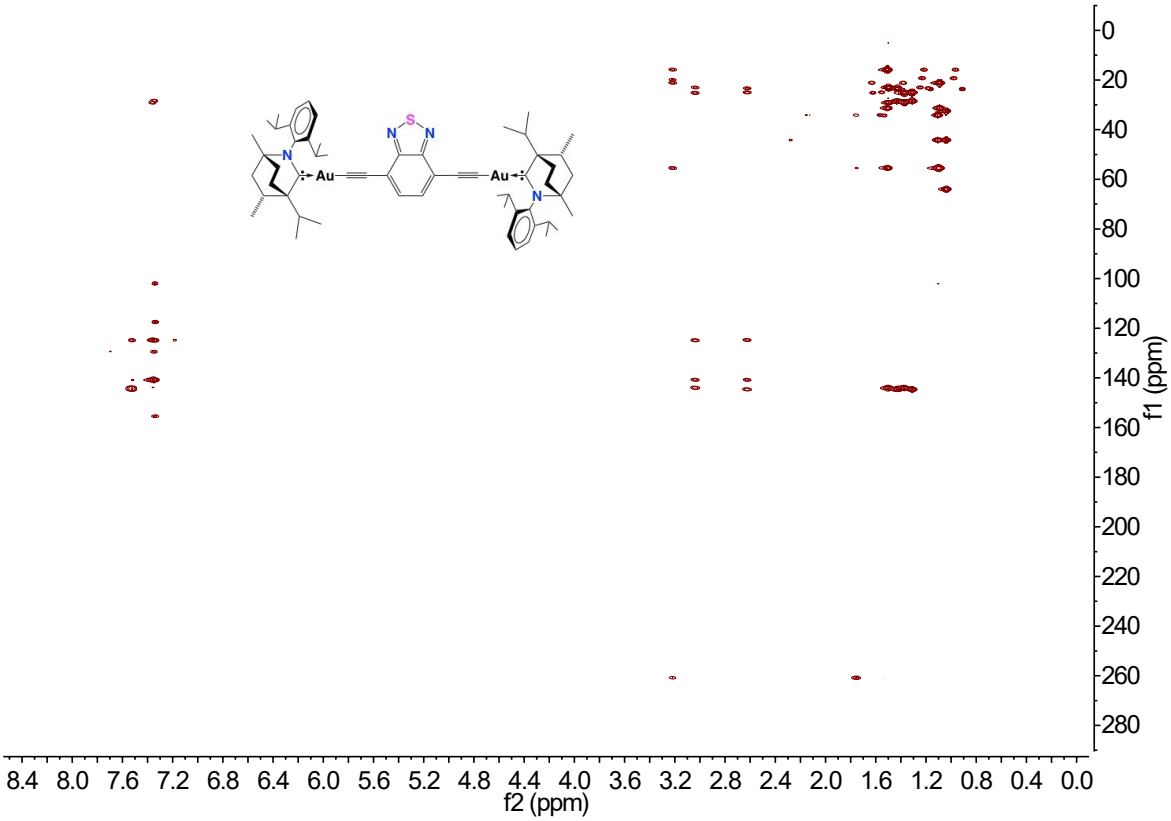

Synthesis of 4-((trimethylsilyl)ethynyl)-2,1,3-benzothiadiazole (L(TMS)1)

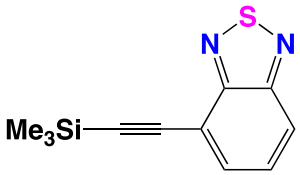

A bomb flask was charged with 4-bromo-2,1,3-benzothiadiazole (2.00 g, 9.30 mmol), CuI (17.7 mg, 93.0 µmol) and $Pd(PPh_3)_2Cl_2$ (65.3 mg, 93.0 µmol) followed by addition of dry THF (45 mL), iPr$_2$NH (45 mL, 321 mmol) and $(CH_3)_3SiC_2H$ (9.01 mL, 65.1 mmol). The resulting suspension was left to stir overnight at 90°C. The reaction mixture was quenched with H_2O (200 mL) and the product extracted with EtOAc (200 mL). The organic phase was dried with excess $MgSO_4$ and filtered. The product was purified via column chromatography (eluent 19:1 hexane:EtOAc). All volatiles were evaporated under reduced pressure to give the product as an orange oil that forms orange crystals on standing in 73% yield (1.57 g, 6.76 mmol). ^{1}H NMR (500 MHz, $CDCl_3$) δ 7.93 (d, J = 8.8 Hz, 1H, BTD), 7.71 (d, J = 6.9 Hz, 1H, BTD), 7.49 (pseudo t, J = 8.4 Hz, 1H, BTD), 0.31 (s, 9H, TMS). ^{13}C NMR (126 MHz, CDCl3) δ 154.52 (C=N BTD, 2xC overlap), 133.55 (BTD), 129.07 (BTD), 122.15 (BTD), 116.99 (BTD), 101.63 (C≡C), 100.15 (C≡C), 0.04 (TMS). IR (ATR, cm^{-1}): 2156 (C≡C). HRMS $C_{11}H_{12}N_2SSi$ theoretical $[M-H]^+$ = 233.0563; HRMS APCI(ASAP) = 233.0561.

L(TMS)1: ^{1}H NMR (500 MHz, $CDCl_3$)

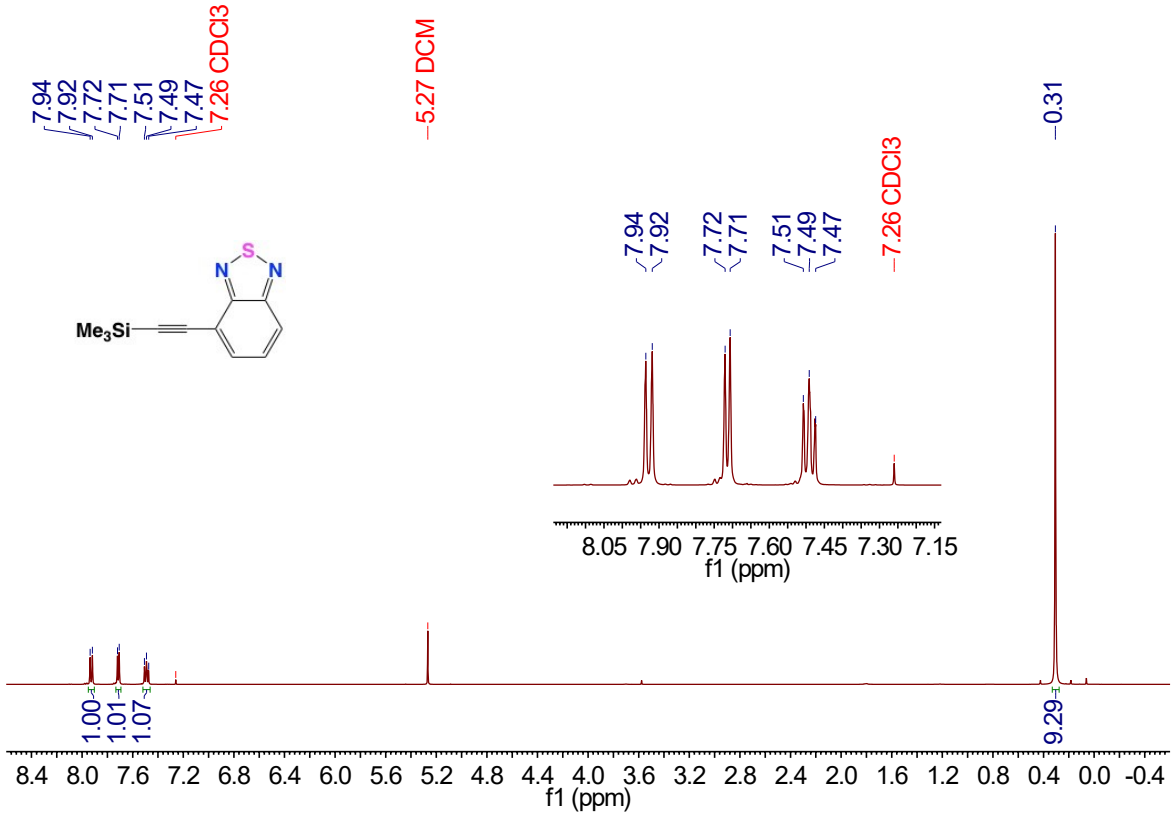

L(TMS)1: ^{13}C{^{1}H} NMR (126 MHz, $CDCl_3$)

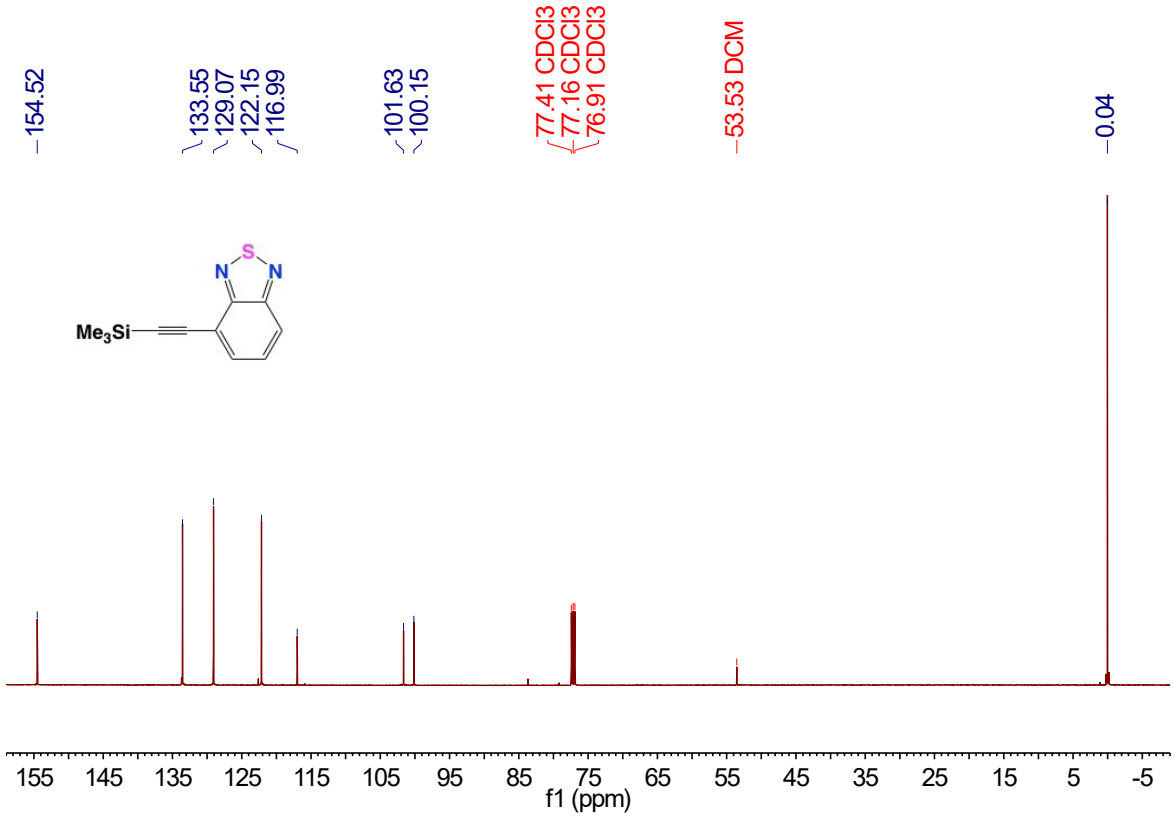

Synthesis of 4-ethynyl-2,1,3-benzothiadiazole (L1)

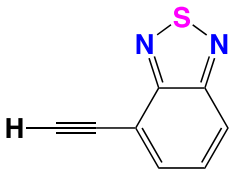

L(TMS)1 (1.10 g, 4.73 mmol) was deprotected by addition of dry THF (15 mL) followed by TBAF (14.2 mL, 14.2 mmol). The reaction mixture was left to stir for 1 h at room temperature. The solution was quenched with dilute HCl (4 wt%, 100 mL) resulting in a colour change from dark green to orange. The solution was washed twice with H_2O (200 mL) and extracted with EtOAc (200 mL). The organic phase was separated, dried over excess $MgSO_4$, and filtered. All volatiles were evaporated to give the product as a pale brown crystalline product in 94% yield (709 mg, 4.43 mmol). ^{1}H NMR (500 MHz, $CDCl_3$) δ 8.04 (d, *J* = 8.8 Hz, 1H, BTD), 7.80 (d, *J* = 6.8 Hz, 1H, BTD), 7.58 (dd, *J* = 8.8, 7.0 Hz, 1H, BTD), 3.59 (s, 1H, C≡C-H). ^{13}C NMR (126 MHz, $CDCl_3$) δ 154.86 (C=N BTD), 154.58 (C=N BTD), 133.84 (BTD), 129.18 (BTD), 122.76 (BTD), 116.05 (BTD), 83.68 (C≡C), 79.29 (C≡C). IR (ATR, cm^{-1}): 2103 (C≡C), 3336 (C≡C-H). HRMS $C_8H_4N_2S$ theoretical $[M-H]^+$ = 161.0168; HRMS APCI(ASAP) = 161.0170.

L1: ^{1}H NMR (500 MHz, $CDCl_3$)

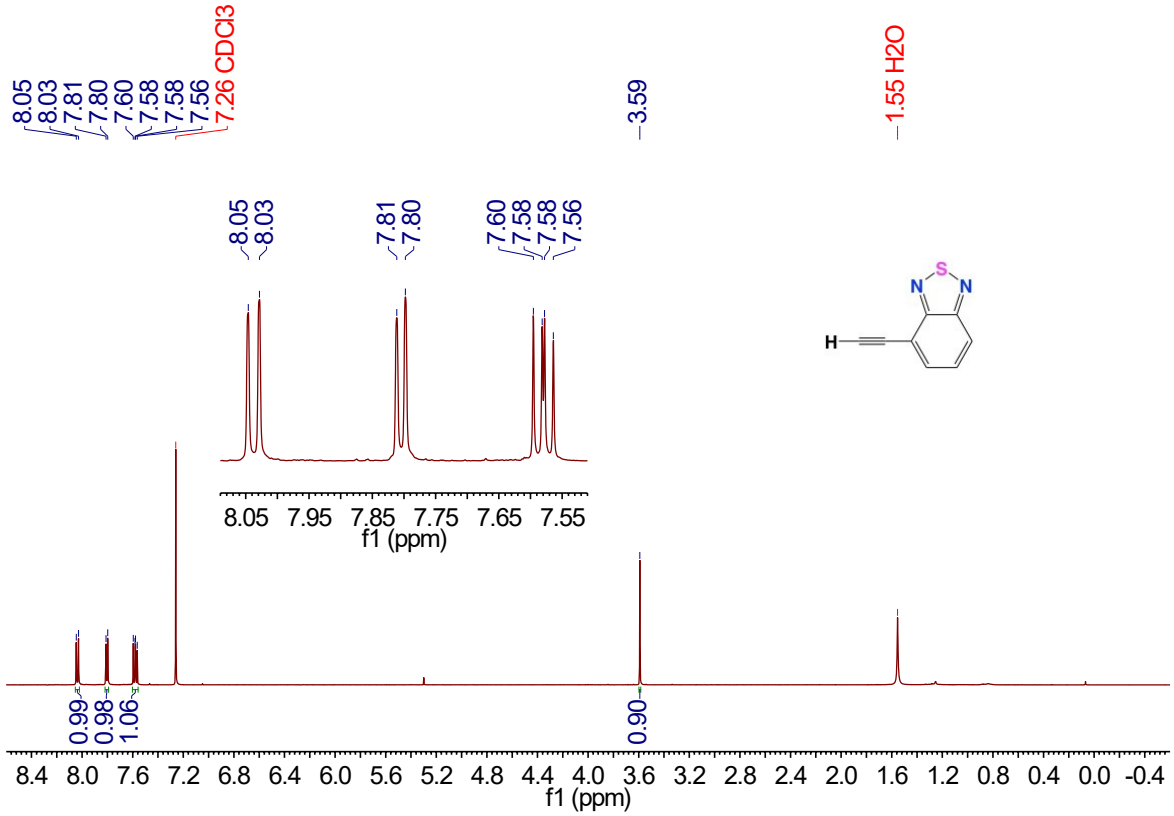

L1: ^{13}C{^{1}H} NMR (126 MHz, $CDCl_3$)

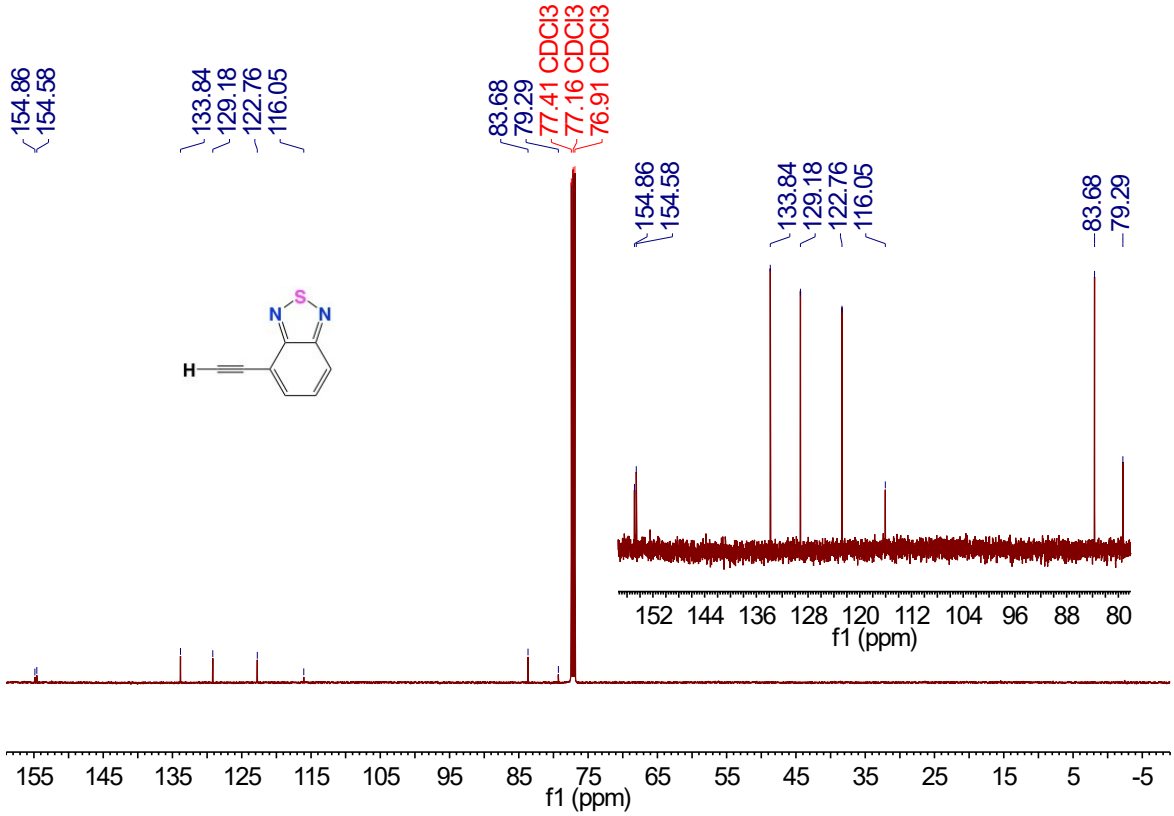

Synthesis of 4,7-di(trimethylsilyl)ethynyl-2,1,3-benzothiadiazole (L(TMS)2)

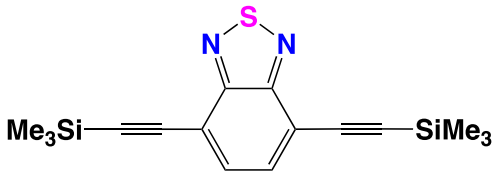

A bomb flask was charged with 4,7-dibromo-2,1,3-benzothiadiazole (2.00 g, 6.80 mmol), CuI (25.9 mg, 136 μmol) and $Pd(PPh_3)_2Cl_2$ (95.5 mg, 136 µmol) followed by addition of dry THF (45 mL), iPr$_2$NH (45 mL, 321 mmol) and $(CH_3)_3SiC_2H$ (13.2 mL, 95.3 mmol). The resulting suspension was left to stir overnight at 90°C. The reaction mixture was quenched with H_2O (200 mL) and the product extracted with EtOAc (200 mL). The organic phase was dried with excess $MgSO_4$ and filtered. The product was purified via column chromatography (eluent 9:1 hexane:EtOAc). All volatiles were evaporated under reduced pressure to give the product as a dark brown crystalline solid in 95% yield (2.13 g, 6.48 mmol). ^{1}H NMR (500 MHz, $CDCl_3$) δ 7.70 (s, 2H, BTD), 0.33 (s, 18H, TMS). ^{13}C NMR (126 MHz, $CDCl_3$) δ 154.36 (C=N BTD), 133.30 (BTD), 117.41 (BTD), 103.79 (C≡C), 100.13 (C≡C), 0.04 (TMS). IR (ATR, cm^{-1}): 2154 (C≡C). HRMS $C_{16}H_{20}N_2SSi_2$ theoretical $[M-H]^+$ = 329.0958; HRMS APCI(ASAP) = 329.0960.

L(TMS)2: ^{1}H NMR (500 MHz, $CDCl_3$)

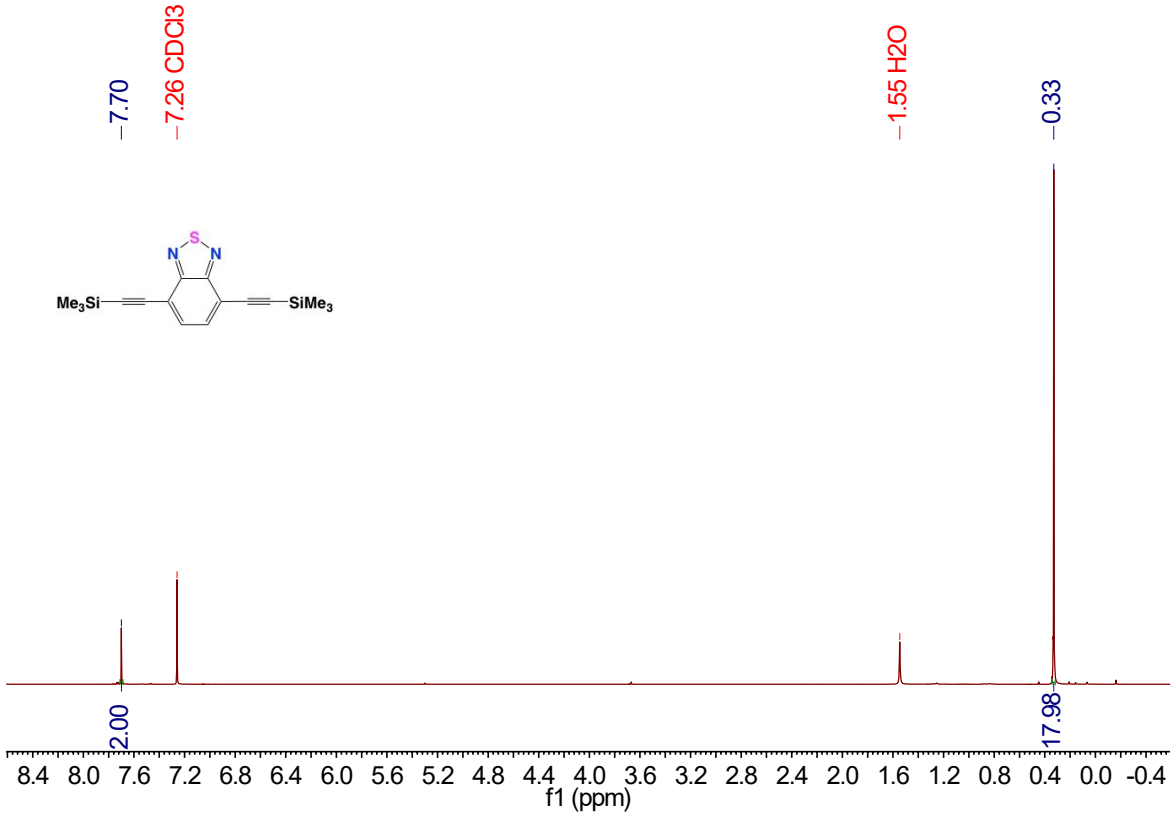

L(TMS)2: ^{13}C{^{1}H} NMR (126 MHz, $CDCl_3$)

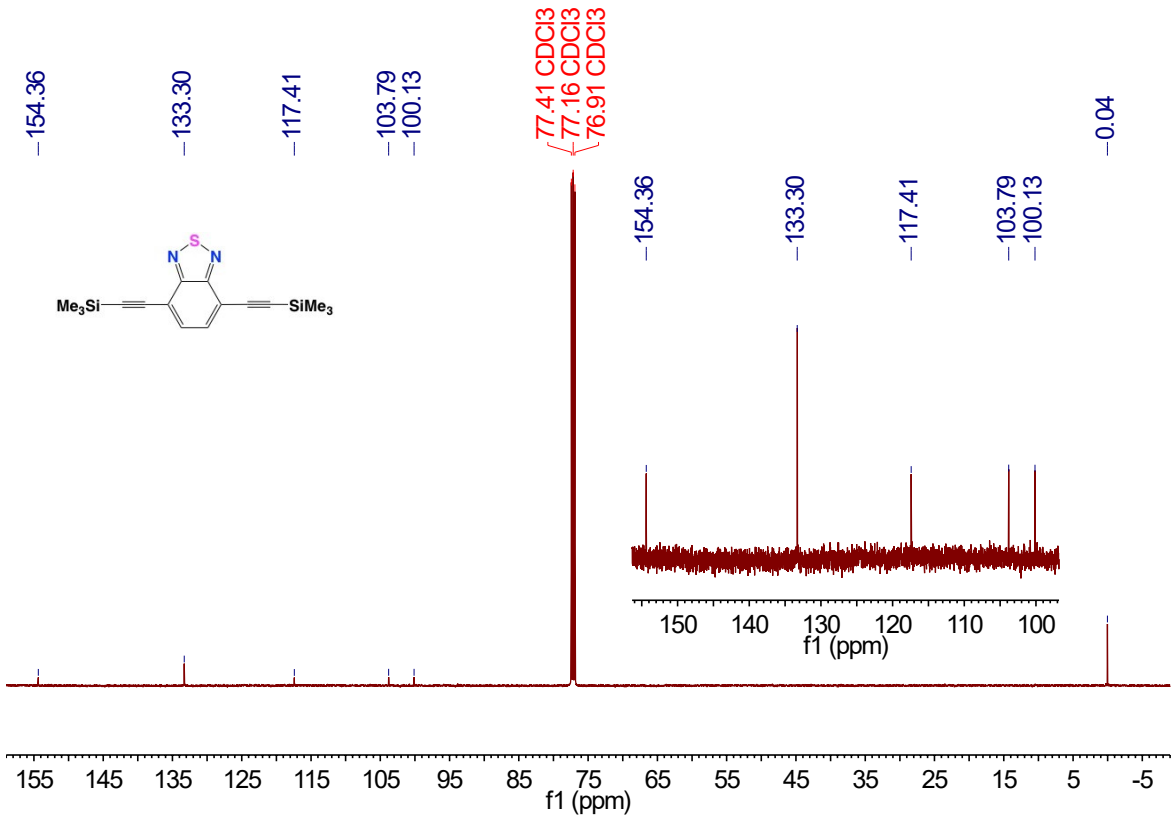

Synthesis of 4,7-diethynyl-2,1,3-benzothiadiazole (L2)

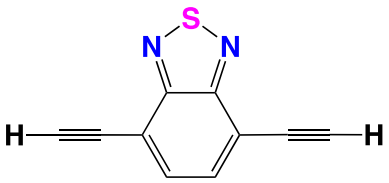

L(TMS)2 (1.10 g, 3.35 mmol) was deprotected by addition of dry THF (15 mL) followed by TBAF (20.1 mL, 20.1 mmol). The reaction mixture was left to stir for 1 h at room temperature. The solution was quenched with dilute HCl (4 wt%, 100 mL). The solution was washed twice with H_2O (200 mL) and extracted with EtOAc (200 mL). The organic phase was separated, dried over excess $MgSO_4$, and filtered. All volatiles were evaporated to give the product dark brown crystalline solid in 80% yield (490 mg, 2.66 mmol). ^{1}H NMR (500 MHz, $CDCl_3$) δ 7.77 (s, 2H, BTD), 3.68 (s, 2H, C≡C-H). ^{13}C NMR (126 MHz, $CDCl_3$) δ 154.50 (C=N BTD), 133.39 (BTD), 116.91 (BTD), 85.49 (C≡C), 79.07 (C≡C). IR (ATR, cm^{-1}): 2105 (C≡C), 3356 (C≡C-H). HRMS $C_{10}H_4N_2S$ theoretical $[M-H]^+$ = 185.0168; HRMS APCI(ASAP) = 185.0171.

L2: ^{1}H NMR (500 MHz, $CDCl_3$)

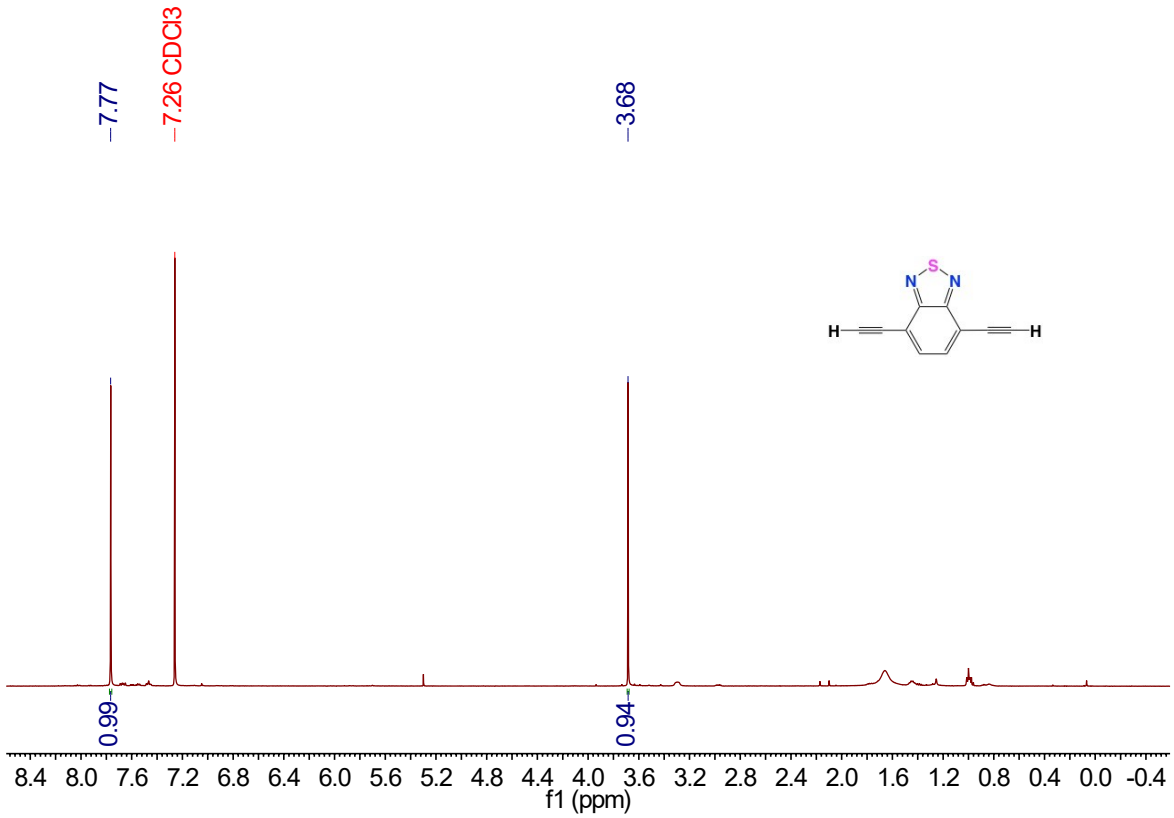

L2: ^{13}C{^{1}H} NMR (126 MHz, $CDCl_3$)

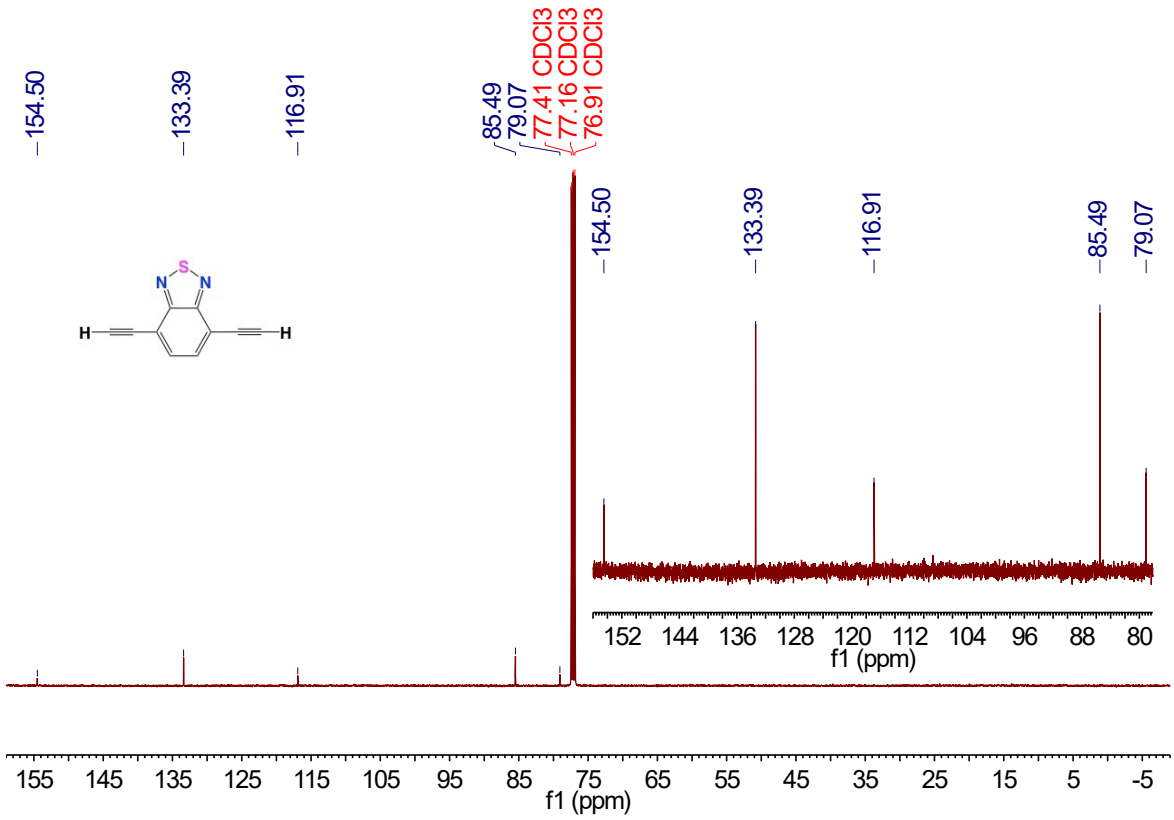

Thermogravimetric Analysis.

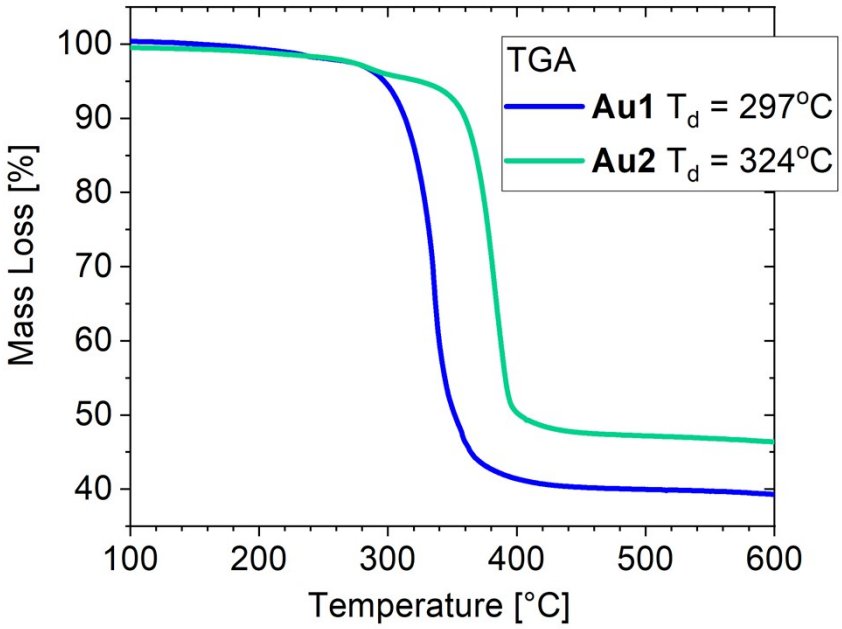

Figure S1. TGA curves for **Au1** and **Au2**. Decomposition temperature (Td) indicates the temperature at 5% weight loss.

Single Crystal X-ray Crystallography.

Crystals suitable for x-ray diffraction study were obtained by slow layer diffusion of hexane into DCM solution at room temperature for **Au1**. Crystals were mounted in oil on glass fiber and fixed on the diffractometer in a cold nitrogen stream. Data was collected using XtaLAB AFC11 (RINC): quarter-chi single diffractometer at 100 K. Data was processed using the CrystAlisPro-CCD and –RED software.[3,4] The 4-ethynyl-2,1,3-benzothiadiazole moiety for complex **Au1** was disordered over two half-populated positions. Multi-scan absorption correction was applied for all crystals. Structures were solved by direct method/intrinsic phasing and refined by the full-matrix least-squares against F^2 in an anisotropic (for non-hydrogen atoms) approximation. All hydrogen atoms were positioned geometrically and constrained to ride on their parent atoms with C-H = 0.95-1.00 Å, and $U_{iso} = 1.2-1.5\ U_{eq}$ (parent atom). All calculations were performed using the SHELXL software[5] and Olex2 graphical user interface.[6]

Principal Crystallographic Data for Au1.

CCDC number: 2351761. $C_{32}H_{40}AuN_3S$ (M =695.69 g/mol), monoclinic, space group $P2_1/n$ (no. 14), a = 11.4448(2) Å, b = 19.0140(2) Å, c = 14.1942(2) Å, β = 108.1460(10)°, V = 2935.20(7) Å^3, Z = 4, T = 100.00(12) K, μ(Mo Kα) = 5.108 mm^{-1}, D_{calc} = 1.574 g/cm^3, 87255 reflections measured (3.702° ≤ 2Θ ≤ 56°), 7084 unique (R_{int} = 0.0301, R_{sigma} = 0.0135) which were used in all calculations. The final R_1 was 0.0360 (I > 2σ(I)) and wR_2 was 0.0878 (all data).

Cyclic Voltammetry.

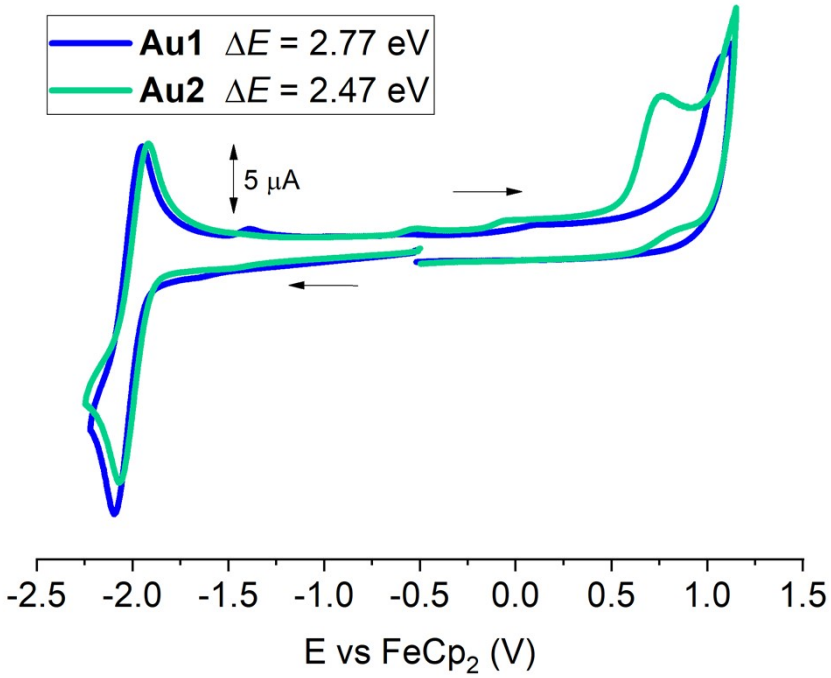

Figure S2. Full range cyclic voltammograms for **Au1** and **Au2**. Recorded using a glassy carbon electrode in THF solution (1.4 mM) with [*n*-Bu_4N]PF_6 as supporting electrolyte (0.13 M), scan rate 0.1 V s^{-1}.

Table S1. Formal electrode potentials (peak position E_p for irreversible and $E_{1/2}$ for quasi-reversible processes (*), *V*, *vs*. $FeCp_2$), onset potentials (*E, V*, *vs*. $FeCp_2$), peak-to-peak separation in parentheses for quasi-reversible processes (ΔE_p in mV), E_{HOMO}/E_{LUMO} (*e*V) and band gap values (ΔE, *e*V) for the redox changes exhibited by **Au1** and **Au2**.[a]

Complex	Reduction		E_{LUMO}	Oxidation		E_{HOMO}	ΔE
	E_{1st}	$E_{onset\ red}$	eV	E_{1st}	$E_{onset\ ox}$	eV	eV
Au1	−2.02* (146)	−1.93	−3.46	+1.06	+0.84	−6.23	2.77
Au2	−1.99* (149)	-1.91	−3.48	+0.76	+0.56	−5.95	2.47

[a] In THF solution, recorded using a glassy carbon electrode, concentration 1.4 m*M*, supporting electrolyte [*n*-Bu_4N][PF_6] (0.13 M), measured at 0.1 V s^{-1}. $E_{HOMO} = -(E_{onset\ ox\ Fc/Fc+} + 5.39)$ *e*V; $E_{LUMO} = -(E_{onset\ red\ Fc/Fc+} + 5.39)$ *e*V (*Adv. Mater.* **2011**, *23*, 2367–2371).

Photophysical Characterisation.

UV-visible absorption spectra were recorded using a Varian Cary 5000 UV-Vis-NIR spectrometer. Photoluminescence measurements were recorded on an Edinburgh Instruments FLS-980 spectrometer with a solids mount attachment where appropriate. Absolute photoluminescence quantum yields were recorded using Hamamatsu Quantaurus-QY C11347-11. Quantum yields have been measured in air for solid samples and under nitrogen for solutions. Time resolved luminescence data were collected on a time-correlated single photon counting (TCSPC) Edinburgh Instruments FLS-980 spectrometer using F-900 software. A xenon flash lamp and EPL pulsed diode lasers were used as excitation sources. The collected data were analysed using F-900 software.

Two-photon absorption (2PA) measurements were performed at NanoMultiPhot (Institute of Molecular Science, Bordeaux university, Talence, France). The 2P were conducted on deaerated solutions of **Au1** and **Au2** in toluene (C= 0.45 mM and 0.17 mM respectively) by two-photon excited fluorescence (TPEF), using fluorescein in aqueous NaOH (C= 0.22 mM, pH= 11.0) as two-photon reference.[7-8] The two-photon absorption experimental setup was measured using the well-established method described by Xu and Webb.[8] An Ultra II (Coherent) femtoseconds pulsed laser (repetition rate: 80 MHz, pulsed width: 150 fs) was focalised on samples or fluorescein solutions using an air Olympus objective (10x, 0.25 NA) under magnetic stirring. Excitation wavelength was tuned in the range 680-960 nm (**Au1**) or 680-1000 nm (**Au2**). The 1 cm quartz cuvette was set in order to have the fluorescence generated on the close vicinity of the wall of the cuvette to limit reabsorption of fluorescence. The fluorescence is then collected in epifluorescence and filtered from back-scattered laser using a dichroic mirror (675dcxru, Chroma) and finally send to a fast spectrophotometer (MayaPro, OceanInsight) by the mean of an optical fiber. The power of the laser is tuned using a polarizer at Brewster's angle (142013, Layertec) in tandem with a rotating halfwave plate. The power is measured in real time by sending a part of the laser beam on a silicon photodiode (S142CL with power meter interface PM101U, both from Thorlabs) using a beam splitter (UFBS5050, Thorlabs). Quadraticity of the TPEF signals is evaluated checking the quadratic dependence of fluorescence to the laser power. The full programs used for TPEF measurements and analysis are available on github.[9] The two-photon brightness $\sigma_2\Phi$ of samples were calculated using equation 2.

$$\sigma_2\Phi = \sigma_2\Phi_{ref} * \left(\frac{n}{n_{ref}}\right)^2 * \frac{C_{ref}}{C} * \left(\frac{\int Fluo.\ int.}{P^2} / \frac{\int Fluo.\ int._{ref}}{P_{ref}^2}\right) * \frac{\eta_{ref}}{\eta}$$

Equation 1. Calculation of two-photon brightness $\sigma_2\Phi$.

Where n is the refractive index, C the concentration, P the laser power, $\int Fluo.\ int.$ The fluorescence intensity and η the spectral correction of the sample and reference (c.a. ref).

UV-Vis and Photoluminescence Spectra

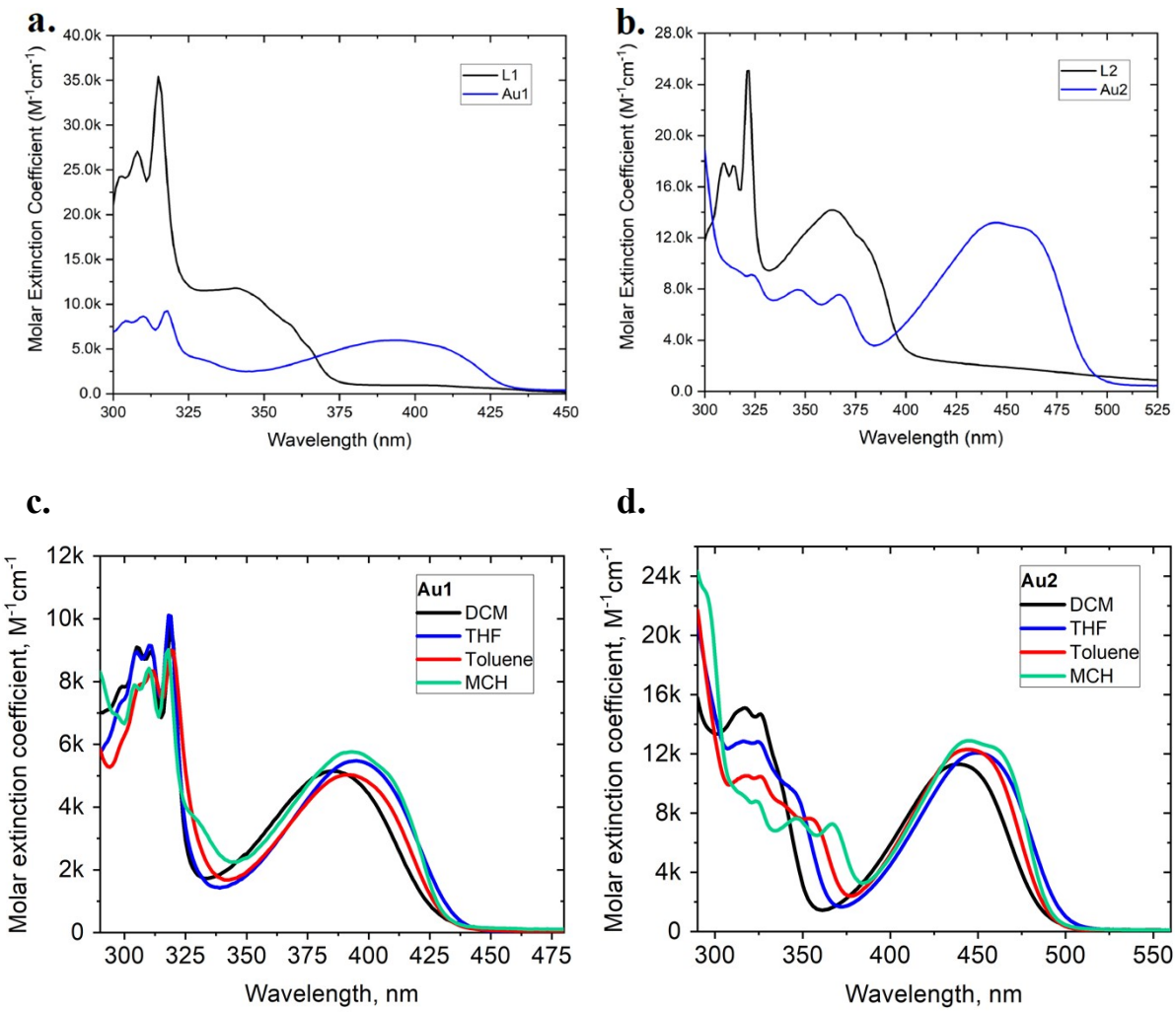

Figure S3. UV-vis spectra for **L1** and **Au1** (a); **L2** and **Au2** (b) in MCH solution. UV-vis absorption spectra of **Au1** (c) and **Au2** (d) in various solvents at 295 K.

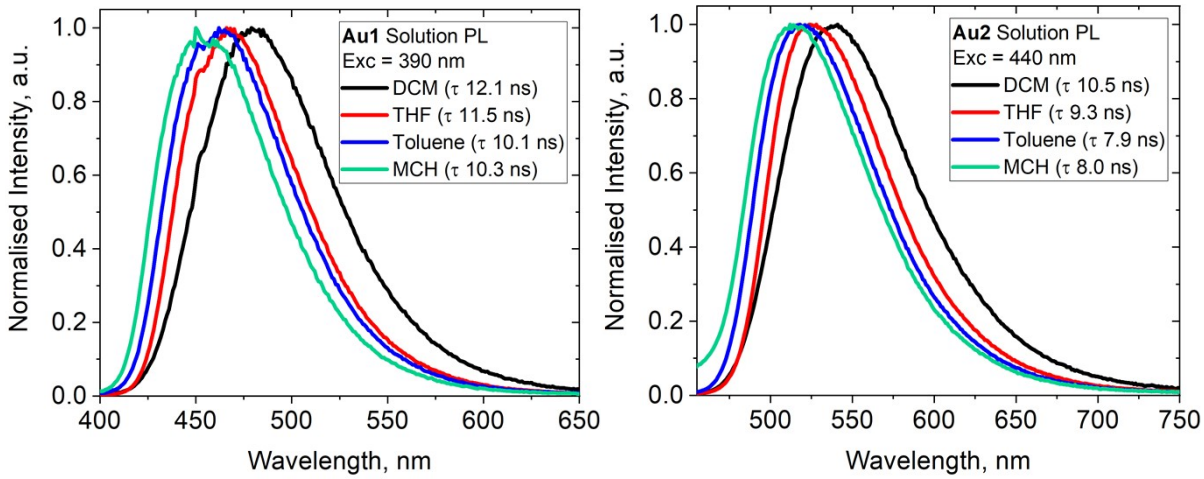

Figure S4. Photoluminescent spectra and emissive lifetimes of **Au1 (**left) and **Au2** (right) in various solvents at 295K.

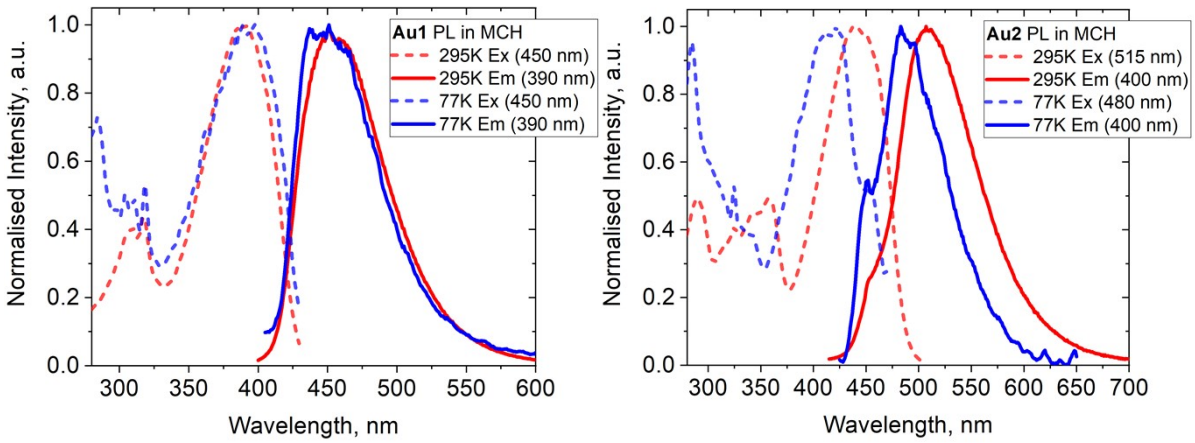

Figure S5. Photoluminescent spectra of **Au1 (**left) and **Au2** (right) in MCH at 295K and 77K.

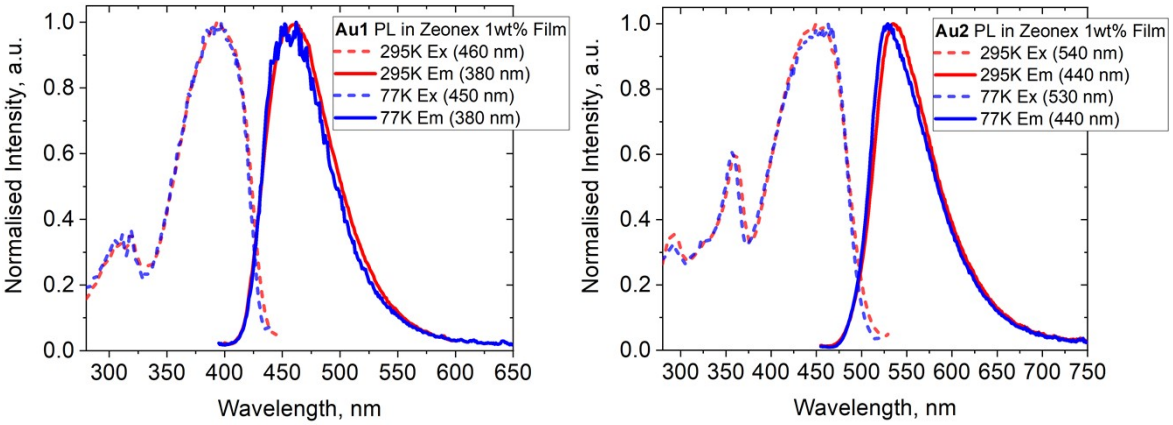

Figure S6. Photoluminescent spectra of **Au1 (**left) and **Au2** (right) in MCH at 295K and 77K.

Table S2. Photophysical properties of complexes **Au1** and **Au2** in methylcyclohexane (MCH).

	λ_{em} (nm)	τ (ns)	Φ (%)[a]	k_r (10^7 s^{-1})[b]	k_{nr} (10^6 s^{-1})[c]	S1 (eV)[d]	λ_{em} (nm, 77K)	τ (ns, 77K)
MCH Solution								
Au1	455	10.3	> 99	9.71	–	3.00	440	8.26
Au2	508	8.04	93	11.6	8.71	2.87	483	6.91

[a] Quantum yields determined using an integrating sphere; [b]radiative rate constant $k_r = \Phi/\tau$; [c] Nonradiative constant $k_{nr} = (1 - \Phi)/\tau$. In case of two-component lifetime τ an average was used: $\tau_{av} = (B_1/(B_1+B_2))\tau_1 + (B_2/(B_1+B_2))\tau_2$, where B_1 and B_2 are the relative amplitudes for τ_1 and τ_2, respectively; [d] S1 energies based on the onset values of the emission spectra blue edge at 77 K and 295 K.

Table S3. Photophysical properties of complexes **Au1** and **Au2** together with corresponding ligands **L1** and **L2** in argon saturated toluene solution.

Compound	$\lambda^{abs, max}$ nm	ε^{max} $M^{-1}.cm^{-1}$	$\lambda^{em, max}$ nm	Φ_f [a]	$2.\lambda^{abs, max}$ nm	$\lambda^{2PA, max}$ nm	σ_2^{max} GM
Au1	391	3 400	458	> 0.99	782	800	0.8
L1	382 447	6 800 500	444	> 0.99	764	740	1
Au2	356 445	10 700 17 500	516	>0.99	712 890	720 820	90 2
L2	420 447	14 400 12 800	467	0.78	840 894	730 880	23 3

[a] *Luminescence quantum yield measured with fluorescein in $NaOH_{aq.}$ (0.1 M, $\Phi_f = 0.9$) as reference.*

2-Photon Absorption

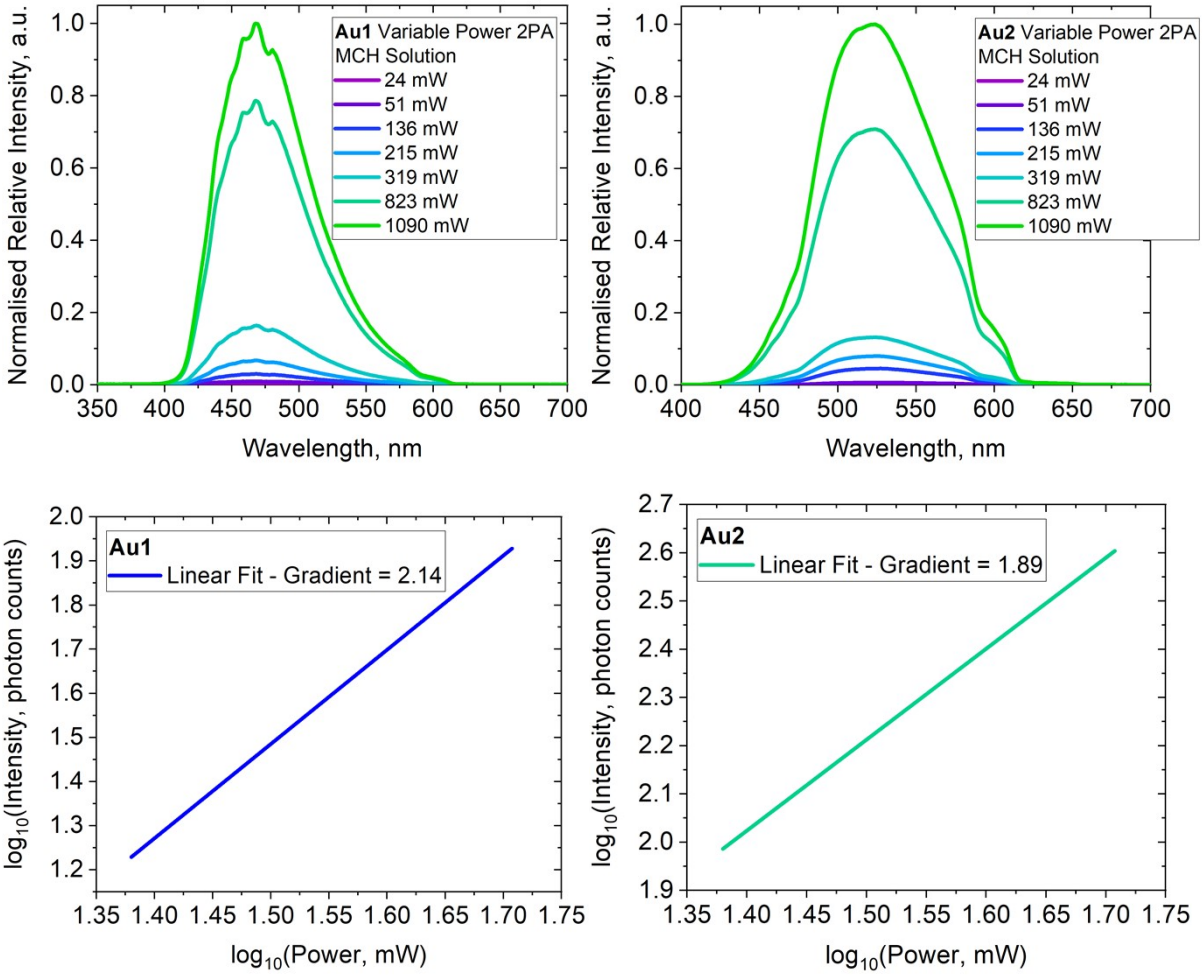

Figure S7. Variable power 2-photon absorption fluorescence spectra of **Au1** (top left) and **Au2** (top right) in MCH solutions. Linear fit plot of $\log_{10}$(laser power) to $1\log_{10}$(PL intensity) with gradients at different power readings from 20 to 100 mW for **Au1** (bottom left) and **Au2** (bottom right) in MCH solutions.

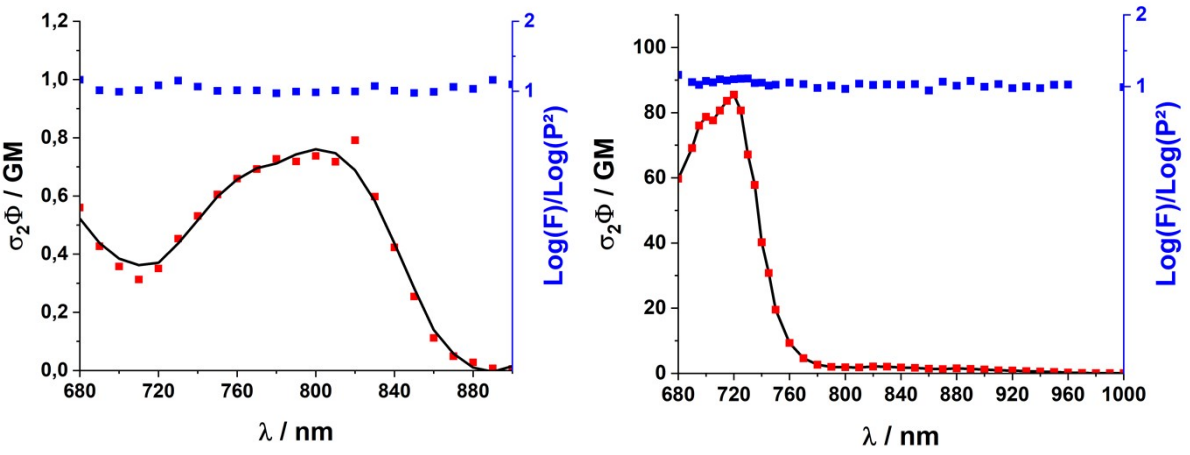

Figure S8. Two-photon brightness (red: experimental, black: smooth) and quadraticity check (Log(F)/Log(P²)) for complexes **Au1** (left) and **Au2** (right) in solutions in deaerated toluene.

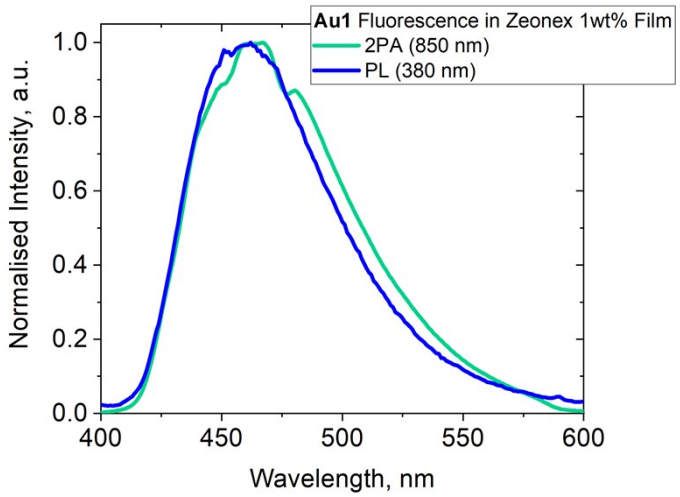

Figure S9. Fluorescence spectra of **Au1** in a Zeonex 1wt% film one-photon excited PL (blue) and two-photon excited PL (green).

a)

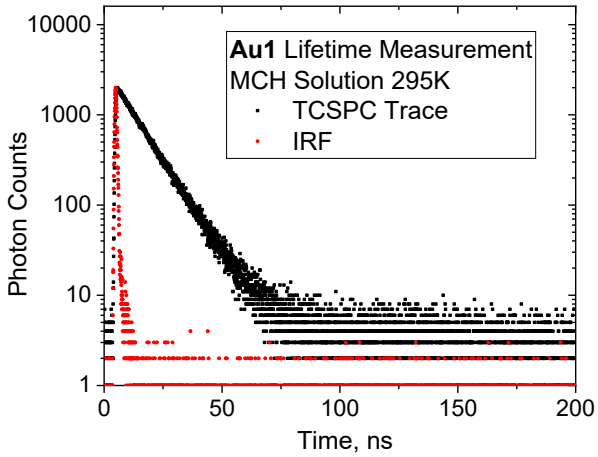
Au1 Lifetime Measurement
MCH Solution 295K
TCSPC Trace
IRF
Photon Counts
Time, ns

b)

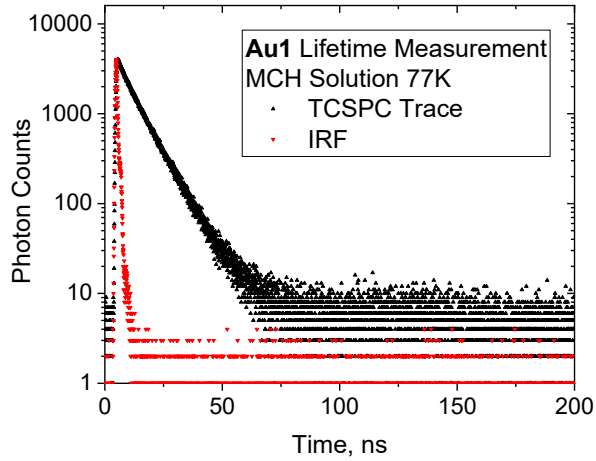
Au1 Lifetime Measurement
MCH Solution 77K
TCSPC Trace
IRF
Photon Counts
Time, ns

c)

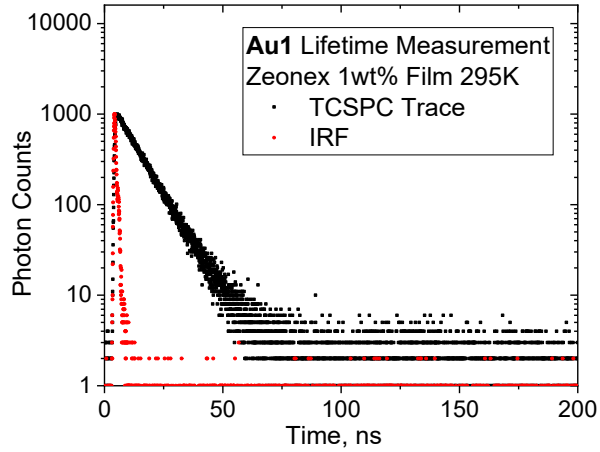
Au1 Lifetime Measurement
Zeonex 1wt% Film 295K
TCSPC Trace
IRF
Photon Counts
Time, ns

d)

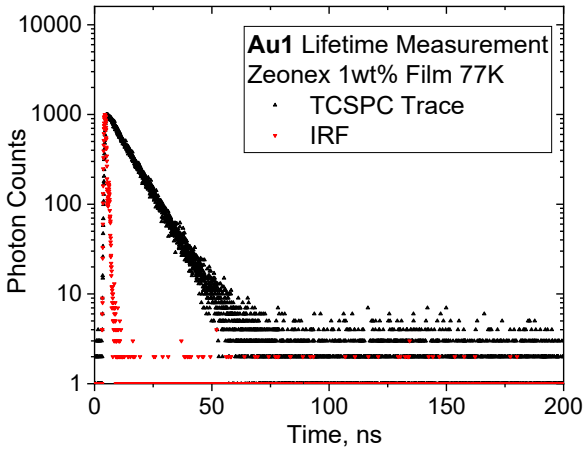
Au1 Lifetime Measurement
Zeonex 1wt% Film 77K
TCSPC Trace
IRF
Photon Counts
Time, ns

e)

f)

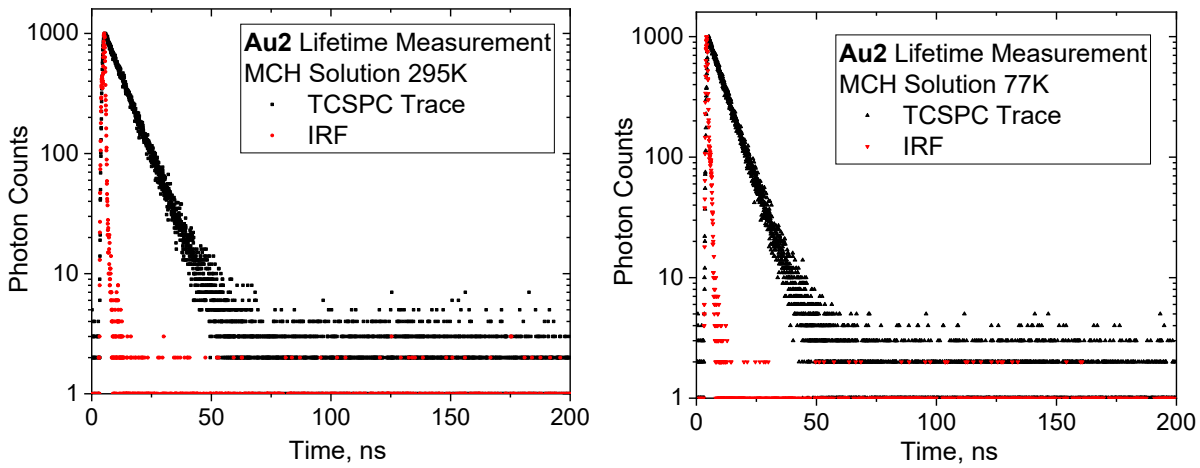

g) **h)**

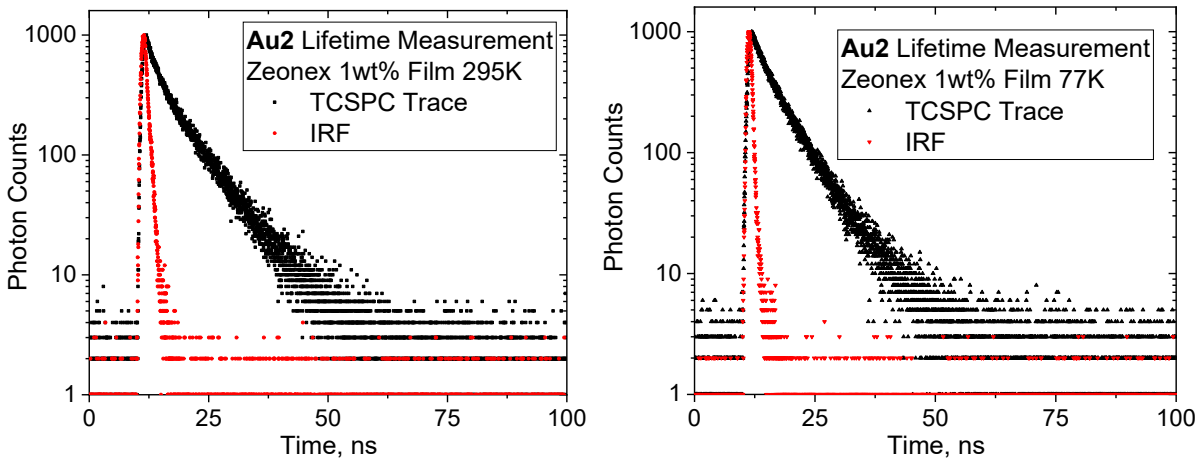

Figure S10. Excited state lifetime traces measured by Time Correlated Single Photon Counting (TSCPC, black) and Instrument Response Function (red) in methylcyclohexane (MCH) solution for complexes **Au1** at 295K (a) and at 77K (b); **Au2** at 295K (e) and at 77K (f); in 1 wt% Zeonex films for **Au1** at 295K (c) and at 77K (d); **Au2** at 295K (g) and at 77K (h).

Computational Calculations

The ground states of the complexes were studied by density functional theory (DFT) and the excited states by time-dependent DFT (TD-DFT) using the Tamm-Dancoff approximation.[10,11] Calculations were carried by the global hybrid MN15 functional of the Minnesota series by Truhlar and coworkers, which has especially good performance for noncovalent interactions and excitation energies.[12] The def2-TZVP basis set[13,14] was employed with relativistic effective core potential of 60 electrons for description of the core electrons of Au.[15] In TD-DFT spin-orbit coupling calculations,[14] an all-electron scalar relativistic SARC-ZORA-TZVP basis set[17] was used for Au. We have previously employed the selected methodology with success for closely related molecules.[18,19] HOMO-LUMO overlap integrals and metal contribution in HOMO and LUMO have been calculated using Multiwfn program.[20] The TD-DFT spin-orbit coupling calculations were carried out by Orca 5.0.3,[21] and all the other calculations using Gaussian 16.[22]

Table S4. Optimised gas phase structures and molecular orbital distribution of the HOMO (middle) and LUMO (right) for complexes **Au1** and **Au2** involved in vertical excitation ($S_0 \rightarrow S_1$), including the contributions of the metal orbitals.

	HOMO	LUMO
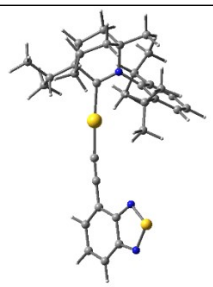 Au1 Overlap integral: 0.68	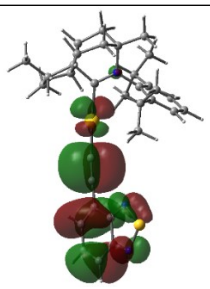 5.8%Au	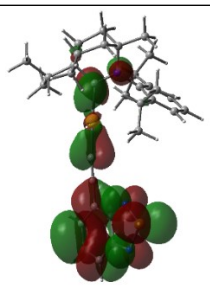 3.8%Au
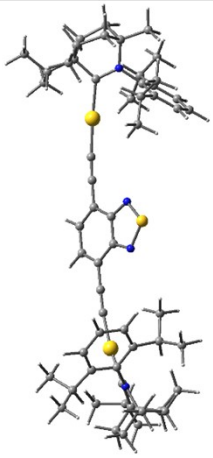 Au2 Overlap integral: 0.67	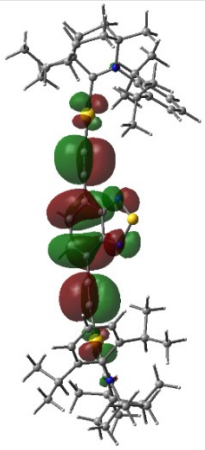 3.0%Au	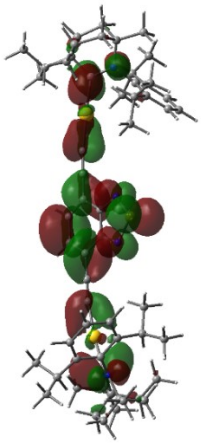 3.8%Au

Table S5. Dipole moments of S_0 and S_n states in S_0 geometry.

	S_0	S_1@S_0	S_2@S_0	S_3@S_0
Au1	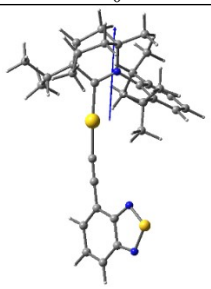 9.0D	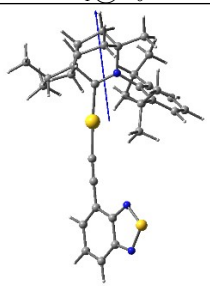 11.1D	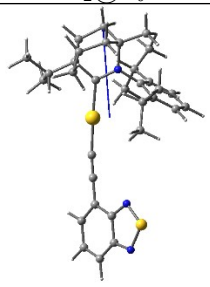 8.9D	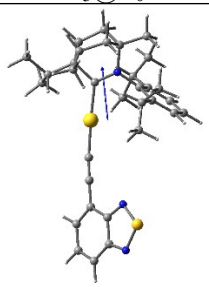 5.4D
Au2	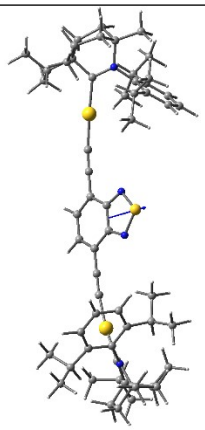 4.5D	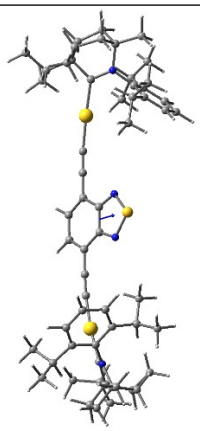 2.3D	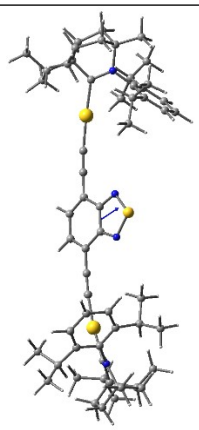 2.5D	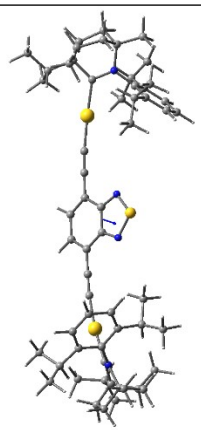 2.0D

Table S6. Theoretically calculated S_n and T_n energy levels, orbital contributions to vertical excitations ($S_0 \rightarrow S_n$ and $S_0 \rightarrow T_n$) and oscillator strength coefficients for complexes **Au1** and **Au2**.

	Excitation energy	Character	Oscillator strength
Au1	S_1 (mixed ^{1}CT and ^{1}LE(A)): 3.41eV = 364nm	HOMO – LUMO (94%)	0.3963
	S_2 (mixed ^{1}CT and ^{1}LE(A)): 3.68eV = 337nm	HOMO-1 – LUMO (58%) HOMO – LUMO+1 (30%)	0.0097
	S_3 (mixed ^{1}CT and ^{1}LE(A)): 3.79eV = 327nm	HOMO – LUMO+1 (56%) HOMO-1 – LUMO (31%)	0.0140
	T_1 (^{3}LE(A)): 2.34eV = 530nm	HOMO – LUMO (83%)	
	T_2 (^{3}LE(A)): 3.42eV = 362nm	HOMO-3 – LUMO (69%)	
	T_3 (mixed ^{3}CT and ^{3}LE(A)): 3.52eV = 352nm	HOMO – LUMO+1 (53%)	
	T_4 (^{3}LE(C+M)): 3.55eV = 349nm	HOMO-2 – LUMO+1 (42%) HOMO-1 – LUMO (17%)	
Au2	S_1 (mixed ^{1}CT and ^{1}LE(A)): 2.94eV = 421nm	HOMO – LUMO (91%)	0.9733
	S_2 (^{1}CT): 3.39eV = 365nm	HOMO – LUMO+1 (83%)	0.0021
	S_3 (mixed ^{1}CT and ^{1}LE(A)): 3.41eV = 364nm	HOMO – LUMO+2 (84%)	0.0225
	T_1 (^{3}LE(A)): 1.99eV = 624nm	HOMO – LUMO (76%)	
	T_2 (mixed ^{3}CT and ^{3}LE(A)): 3.20eV =	HOMO – LUMO+2 (67%)	

	387nm		
	T_3 (^{3}CT): 3.20eV = 387nm	HOMO – LUMO+1 (75%)	
	T_4 (^{3}LE(A)): 3.43eV = 361nm	HOMO-6 – LUMO (59%) HOMO-6 – LUMO+2 (27%)	

A: Acetylide ligand; M: Metal; C: Carbene ligand

Table S7. Natural transition orbitals for S_n and T_n states of gold complexes **Au1** and **Au2** (n = 1, 2, 3).

		HONTO	LUNTO
Au1	S_1	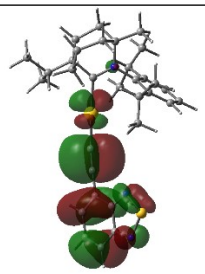	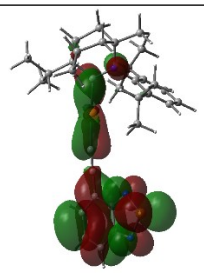
	S_2	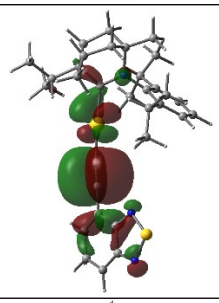	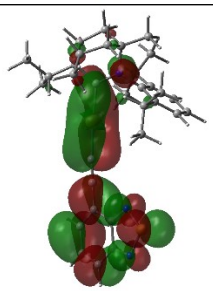
	S_3	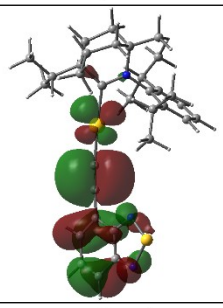	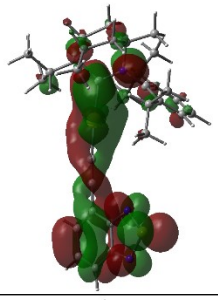
	T_1	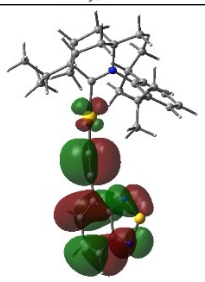	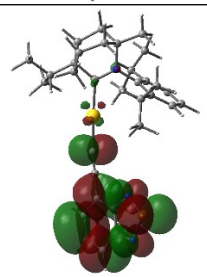
	T_2	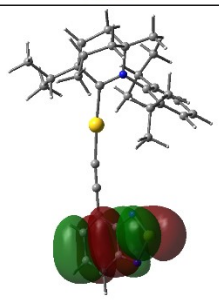	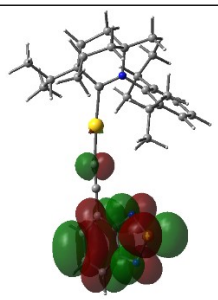

	T_3	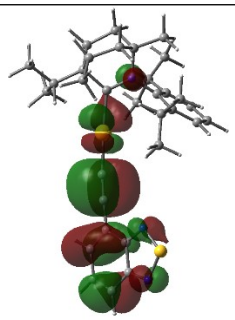	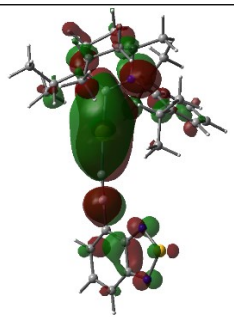
	T_4	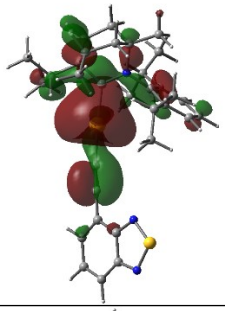	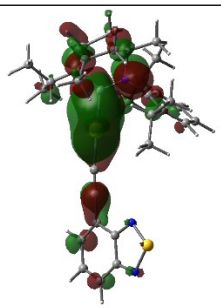
Au2	S_1	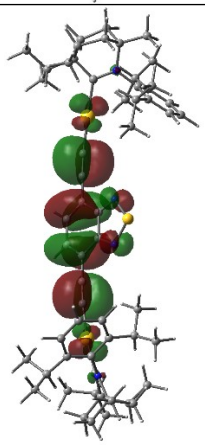	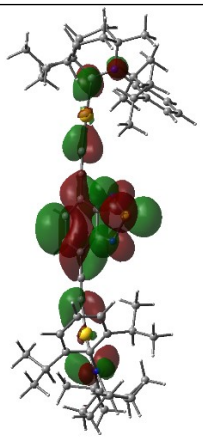
	S_2	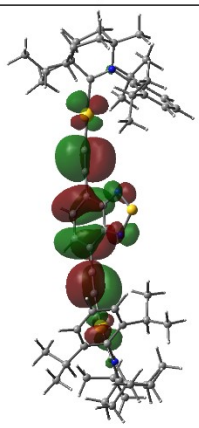	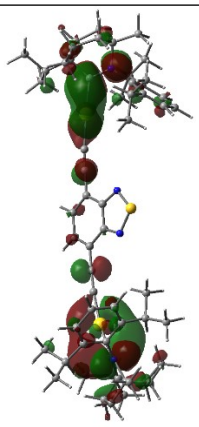

	S_3	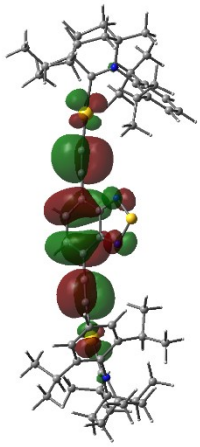	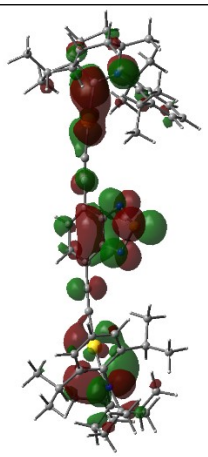
	T_1	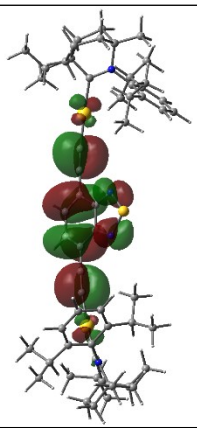	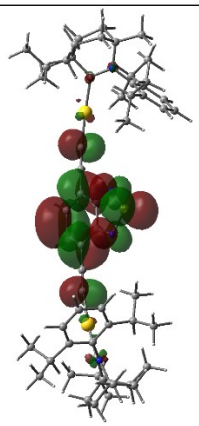
	T_2	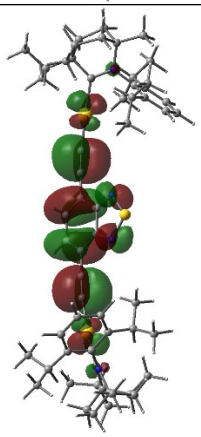	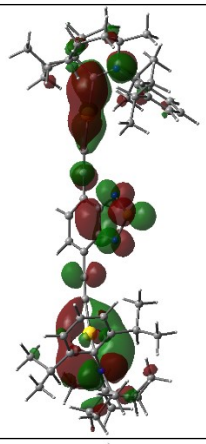
	T_3	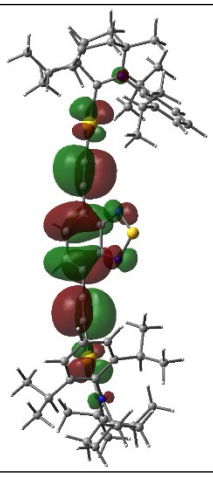	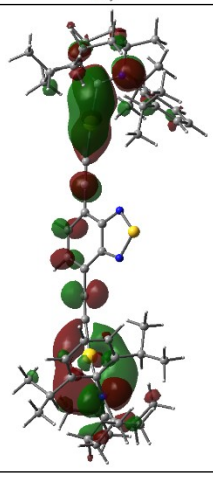

	T_4	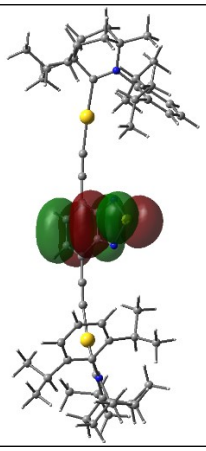	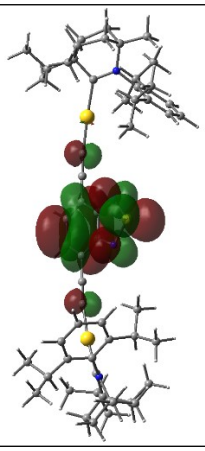

Table S8. Spin orbit coupling matrix elements (SOCME, cm^{-1}) between triplet and singlet states for complexes **Au1** and **Au2**.

	State		Component		
	T	S	Z	X	Y
Au1	1	0	-5.73	7.16	-11.17
	1	1	2.59	27.92	5.40
	1	2	-24.54	75.75	-29.06
	2	0	21.20	-11.04	57.43
	2	1	-3.55	33.29	-2.74
	2	2	5.85	-52.84	8.11
Au2	1	0	0.00	-8.48	16.27
	1	1	5.63	0.00	0.00
	1	2	0.00	-14.67	-115.66
	2	0	221.70	0.00	0.00
	2	1	0.00	6.48	109.92
	2	2	60.03	0.00	0.00

Spin orbit coupling matrix elements (SOCME, cm^{-1}) between T_{1-10} and S_1 for complexes **Au1** and **Au2**.

	State		Component		
	T	S	Z	X	Y
Au1	1	1	2.59	27.92	5.40
	2	1	-3.55	33.29	-2.74
	3	1	-268.46	-196.10	-183.70
	4	1	-43.08	137.66	-30.48
	5	1	167.54	-296.24	132.25
	6	1	-17.48	-164.59	-17.24
	7	1	48.70	-20.28	22.65
	8	1	-119.18	88.28	-95.13
	9	1	47.52	50.49	34.74
	10	1	-459.21	-120.28	-353.21
Au2	1	1	5.63	0.00	0.00
	2	1	0.00	6.48	109.92
	3	1	0.35	0.00	0.00
	4	1	0.00	-3.35	-61.45
	5	1	-273.79	0.00	0.13
	6	1	0.19	2.31	183.31

	7	1	0.00	6.38	301.84
	8	1	-238.77	0.00	0.00
	9	1	0.00	8.57	164.20
	10	1	8.67	0.00	0.00

Table S9. Mixed SOC-states for complexes **Au1** and **Au2**.

	State	Energy / eV	Character[a]	Oscillator strength	Transition electric dipole moment			
					T^2	T_x (au)	T_y (au)	T_z (au)
Au1	0	0.00	$\mathbf{S_0}$ 100%					
	1	2.33	T_1 100%	0.0000	0.0000	0.0053	0.0015	0.0001
	2	2.33	T_1 100%	0.0000	0.0000	0.0020	0.0023	0.0006
	3	2.33	T_1 100%	0.0000	0.0001	0.0025	0.0039	0.0082
	4	3.36	T_3 46% T_2 27% T_4 14%	0.0190	0.2306	0.4802	0.0001	0.0042
	5	3.36	T_3 39% T_2 36% T_4 20%	0.0050	0.0612	0.2473	0.0077	0.0015
	6	3.37	$\mathbf{S_1}$ 47% T_3 26% T_2 15%	0.1894	2.2962	1.5150	0.0246	0.0195
	7	3.39	T_2 87%	0.0004	0.0052	0.0618	0.0124	0.0348
	8	3.41	T_2 58% T_3 30%	0.0001	0.0008	0.0273	0.0014	0.0021
	9	3.42	T_2 40% T_3 22% $\mathbf{S_1}$ 19% T_4 11%	0.0838	0.9997	0.9997	0.0030	0.0168
	10	3.43	T_3 47% T_2 20% T_5 13% $\mathbf{S_1}$ 12%	0.0357	0.4255	0.6516	0.0305	0.0056
	11	3.46	T_4 79% T_2 11%	0.0007	0.0088	0.0846	0.0123	0.0389
	12	3.47	T_4 60% T_5 19% T_3 10%	0.0001	0.0011	0.0334	0.0004	0.0016
	13	3.51	T_4 53% T_3 27%	0.0424	0.4927	0.7000	0.0108	0.0504
	14	3.57	T_5 68% $\mathbf{S_2}$ 12%	0.0149	0.1699	0.3968	0.0146	0.1107
	15	3.62	T_5 68% T_3 12%	0.0089	0.1008	0.3130	0.0529	0.0042
	16	3.65	T_5 71% T_3 14% T_4 10%	0.0002	0.0024	0.0485	0.0036	0.0027
	17	3.69	$\mathbf{S_2}$ 67% T_5 15%	0.0032	0.0352	0.1826	0.0332	0.0265
	18	3.76	$\mathbf{S_3}$ 76%	0.0076	0.0828	0.2791	0.0688	0.0145
Au2	0	0.00	$\mathbf{S_0}$ 100%					
	1	2.06	T_1 100%	0.0000	0.0000	0.0000	0.0000	0.0013
	2	2.06	T_1 100%	0.0000	0.0000	0.0000	0.0000	0.0021

	3	2.06	T_1 100%	0.0000	0.0001	0.0081	0.0074	0.0000
	4	2.99	**S_1** 98%	0.9740	13.2955	0.0293	3.6462	0.0000
	5	3.17	T_2 90%	0.0000	0.0001	0.0074	0.0033	0.0000
	6	3.17	T_2 92%	0.0007	0.0085	0.0079	0.0918	0.0000
	7	3.18	T_2 78% T_3 17%	0.0001	0.0009	0.0000	0.0000	0.0301
	8	3.18	T_3 93%	0.0000	0.0000	0.0000	0.0000	0.0052
	9	3.19	T_3 77% T_2 18%	0.0000	0.0002	0.0000	0.0000	0.0129
	10	3.19	T_3 93%	0.0006	0.0072	0.0570	0.0630	0.0000
	11	3.36	**S_2** 52% T_6 31% T_5 11%	0.0008	0.0097	0.0000	0.0000	0.0985
	12	3.38	T_5 47% **S_3** 36%	0.0002	0.0020	0.0229	0.0379	0.0000
	13	3.40	T_4 52% T_6 35%	0.0000	0.0000	0.0010	0.0013	0.0000
	14	3.41	T_4 87%	0.0002	0.0027	0.0043	0.0515	0.0000
	15	3.41	T_5 67% T_7 13%	0.0000	0.0000	0.0000	0.0000	0.0009
	16	3.41	T_4 88%	0.0000	0.0000	0.0000	0.0000	0.0031
	17	3.42	T_4 48% T_6 37% T_8 10%	0.0000	0.0000	0.0003	0.0046	0.0000
	18	3.43	T_6 28% T_5 24% **S_3** 23%	0.0009	0.0113	0.0126	0.1056	0.0000
	19	3.43	T_6 42% T_5 20% **S_2** 15% T_8 15%	0.0000	0.0003	0.0000	0.0000	0.0184
	20	3.48	T_5 59% **S_2** 24%	0.0022	0.0254	0.0000	0.0000	0.1594
	21	3.48	T_6 46% **S_3** 35%	0.0325	0.3804	0.0029	0.6167	0.0000

[a] >10% contributions

References

[1] F. Chotard, V. Sivchik, M. Linnolahti, M. Bochman, A. S. Romanov, Chem. Mater. 2020, **32**, 14, 6114–6122

[2] G. Gritzner, J. Kůta, *Electrochim. Acta*, 1984, **29**, 869−873.

[3] Programs CrysAlisPro, Oxford Diffraction Ltd. Abingdon, UK, 2010.

[4] G. Sheldrick, *Acta Cryst. C* 2015, **71** (1), 3-8.

[5] G. Sheldrick, *Acta Cryst. A* 2015, **71** (1), 3-8.

[6] O. V. Dolomanov, L. J. Bourhis, R. J. Gildea, J. A. K. Howard, H. Puschmann, *J. Appl. Cryst.* 2009, **42** (2), 339-341.

[7] M. A. Albota, C. Xu, W. W. Webb, *Appl. Opt.*, 1998, **37** (31), 7352.

[8] C. Xu, W. W. Webb, *J. Opt. Soc. Am. B*, 1996, **13** (3), 481.

[9] J. Daniel, website link: https://github.com/LAGONteam/PyTwoPhotonExcitedFluorescence.

[10] F. Furche and D. Rappoport, M. Olivuccim, Ed.; Elsevier: Amsterdam, 2005; 93–128.

[11] G. M. J. Peach and D. J. Tozer, *J. Phys. Chem. A,* 2012, **116**, 9783–9789.

[12] H. S. Yu, X. He, S. L. Li and D. G. Truhlar, *Chem. Sci*., 2016, **7**, 5032–5051.

[13] F. Weigend, M. Häser, H. Patzelt and R. Ahlrichs, *Chem. Phys. Lett.,* 1998, **294**, 143–152.

[14] F. Weigend and R. Ahlrichs, *Phys. Chem. Chem. Phys.,* 2005, **7**, 3297–3305.

[15] D. Andrae, U. Haeussermann, M. Dolg, H. Stoll and H. Preuss, *Theor. Chim. Acta*, 1990, **77**, 123–141.

[16] B. de Souza, G. Farias, F. Neese, R. Izsák, *J. Chem. Theory Comput.* **2019**, *15*, 1896-1904.

[17] D. A. Pantazis, X.-Y. Chen, C. R. Landis, F. Neese, *J. Chem. Theory Comput.* **2008**, *4*, 908-919.

[18] F. Chotard, A. S. Romanov, D. L. Hughes, M. Linnolahti and M. Bochmann, *Eur. J. Inorg. Chem.,* 2019, 4234–4240.

[19] A. S. Romanov, S. T. E. Jones, Q. Gu, P. J. Conaghan, B. H. Drummond, J. Feng, F. Chotard, L. Buizza, M. Foley, M. Linnolahti, D. Credgington and M. Bochmann, *Chem. Sci*., 2020, **11**, 435–446.

[20] T. Lu and F. J. Chen, *Comput. Chem*., 2012, **33**, 580–592.

[21] F. Neese, *WIREs Comput. Mol. Sci.* **2022**, *12*, e1606.

[22] Gaussian 16, Revision A.03, M.J. Frisch, G.W. Trucks, H.B. Schlegel, G.E. Scuseria, M.A. Robb, J.R. Cheeseman, G. Scalmani, V. Barone, G.A. Petersson, H. Nakatsuji, X. Li, M.

Caricato, A.V. Marenich, J. Bloino, B.G. Janesko, R. Gomperts, B. Mennucci, H.P. Hratchian, J.V. Ortiz, A.F. Izmaylov, J.L. Sonnenberg, D. Williams-Young, F. Ding, F. Lipparini, F. Egidi, J. Goings, B. Peng, A. Petrone, T. Henderson, D. Ranasinghe, V.G. Zakrzewski, J. Gao, N. Rega, G. Zheng, W. Liang, M. Hada, M. Ehara, K. Toyota, R. Fukuda, J. Hasegawa, M. Ishida, T. Nakajima, Y. Honda, O. Kitao, H. Nakai, T. Vreven, K. Throssell, J.A. Montgomery, Jr., J.E. Peralta, F. Ogliaro, M.J. Bearpark, J.J. Heyd, E.N. Brothers, K.N. Kudin, V.N. Staroverov, T.A. Keith, R. Kobayashi, J. Normand, K. Raghavachari, A P. Rendell, J.C. Burant, S.S. Iyengar, J. Tomasi, M. Cossi, J.M. Millam, M. Klene, C. Adamo, R. Cammi, J.W. Ochterski, R.L. Martin, K. Morokuma, O. Farkas, J.B. Foresman and D.J. Fox, Gaussian, Inc., Wallingford CT, 2016.